TALLINN UNIVERSITY OF TECHNOLOGY
School of Information Technologies

Gabriel Villers 163538IVEM

RT-Box Controlled Laboratory Test Bench for Teaching Super Capacitor Properties

Master's thesis

Supervisor: Indrek Roasto
PhD
Co-supervisor: Olev Märtens
PhD

Tallinn 2021

TALLINNA TEHNIKAÜLIKOOL
Infotehnoloogia teaduskond

Gabriel Villers 163538IVEM

RT-Box'i juhtimisega katsestend ülikondensaatorite omaduste õpetamiseks

Magistritöö

Juhendaja: Indrek Roasto
PhD
Kaasjuhendaja: Olev Märtens
PhD

Tallinn 2021

Author’s declaration of originality

I hereby certify that I am the sole author of this thesis. All the used materials, references to the literature and the work of others have been referred to. This thesis has not been presented for examination anywhere else.

Author: Gabriel Villers

10.05.2021

Abstract

The increasing use of renewable energy and electric or hybrid vehicles has also led to an increased usage of DC buses. This demands engineers to keep developing and maintaining the systems where Supercapacitors, as high power density components, are capable of compensating rapid changes of power on DC buses.

The main goal of this work was to build a supercapacitor energy storage test bench for teaching. It was built using modern IT tools, so the model of the converters control part was made using PLECS software, using visual building blocks. The bench hardware is driven by RT-Box, which holds and runs the uploaded converter controller model.

This work gives an overview of existing base bi-directional DC-DC converter topologies, more detail of used Half-bridge converter which is commonly used topology. The main nodes of models and their functions are described as the base steps to tune the model with real hardware.

Although the set goals were not achieved in terms of power, voltages and currents, the prepared test bench for educational purposes has been tested with the control system model and the performance has been shown.

This thesis is written in English and is 56 pages long, including 6 chapters, 35 figures and 3 tables.

Annotatsioon

RT-Box’i juhtimisega katsestend ülikondensaatorite omaduste õpetamiseks

Tänapäevane elektritranspordi ja taastuvenergia võrkude suurenev levik, on muutunud ka alalispinge siinide kasutamise järjest laialdasemaks. Ülikondensaatorid, oma üldtuntud suure võimsustihedusega, on heaks täienduseks aeglaste või piiratud võimsusega energiaallikate ja salvestite, tarbitava või genereeritava energia kiiretoimeliseks kompenseerimiseks.

Seetõttu on vajadus ülikondensaatorite teadmistega inseneride koolitamisele ka TalTechi Inseneriteaduskonnas, mistõttu on vastava õppestendi olemasolu vajalik.

Töös on antud ülevaade ülikondensaatorite põhiomadustest, võrrelduna laialt levinud akudega ning alternatiivse suure võisustihedusega salvesti hooratastega. Samuti on käsitletud ülikondensaatorite eripärast tulenevatest nõuetest muunduritele. on antud ülevaade DC-DC muundurite põhiskeemide kahesuunalistest versioonidest ning nende kasutamisest suure võimsusega seadmetes. Samuti on tutvustatud üksikute konverterite paralleelset ühendamist ühtseks, mitme faasiliseks konverteriks, millel on suurem summaarne võimsus ja paremad pulsatsiooni näitajad.

Täpsemalt on kirjeldatud enamlevinud poolsild muundurit, selle eripärasid, arvutuskäiku ning häälestust praktikas.

Töö peamiseks eesmärgiks on luua ülikondensaatorite katsestend sobiva muunduriga. Selleks on olemasolev katsestend ümber ehitatud ning muudetud RT-Box’iga juhitavaks. Samuti valmis töö käigus vajalik juhtimismudel PLECS keskkonnas, mis on sobiv RT-Box’i laadimiseks.

Mudeli loomisel on silmas peetud õppeotstarbelisust, mistõttu pole kasutatud C koodi vaid ainult visuaalseid mudeli komponente. Samuti on mudeli erinevad funktsionaalsused

nagu kaitse ja juhtloogika, jagatud intuitiivselt arusaadavateks mooduliteks, mida oleks erinevate õppetöö osade käigus lihtne kohandada või muuta.

Kuna stendi ehitusel on kasutatud peamiselt juba olemasolevaid komponente, siis selgus töö käigus ühtlasi, et komponentide omavaheline kokkusobivus ei võimalda realiseerida üksikkomponentide täielikku potentsiaali. Nii jäi soovitud alalispinge siini optimaalseks pingeks 200 V ja ning superkondensaatorite laadimis ja tühjenemise vooluks 10 A andes võimsuseks kuni 1 kW.

Mudeli toimivus on katsestendis testitud, ülikondensaatori laadimis- ja tühjenemispingete piirangud on toimivad ning muundur hoiab pinged 10% piires. Kuna stend on ennekõike õppeotstarbeline, siis on püstitatud lõppvõimsuse mittesaavutamine, nii komponentide täiendava ressursi, kui ka alanenud pingete, voolude ja võimsuste tõttu suurema turvalisuse näol, täiesti aktsepteeritav.

Lõputöö on kirjutatud inglise keeles ning sisaldab teksti 56 leheküljel, 6 peatükki, 35 joonist, 3 tabelit.

List of abbreviations and terms

DC	Direct current
AC	Alternate current
PV	Photovoltaic
FC	Fuel Cells
SC	Supercapacitor
FW	Flywheel
BDC	Bi-Directional Converter
SoC	State-of-Charge
PI	Proportional-Integral
D	Duty Cycle
PWM	Pulse Width Modulation

Table of contents

List of figures

List of tables

1 Introduction

The increasing use of renewable energy and electric or hybrid vehicles in the contemporary world has also led to an increased usage of DC buses. This demands engineers to keep constantly developing and maintaining the mentioned systems. Energy sources usually used DC systems such as Photovoltaic (PV) panels in renewable energy, Fuel Cells (FC) especially in transportation, have limited power and reaction time for load change capabilities and thus need to be accompanied with fast response energy saving systems based on Super Capacitors (SC) or Flywheel (FW) technologies. The overview of most used energy stored devices used based on [1] gathered into Table 1.

Table 1 Overview of most used energy storing devices

Function	Supercapacitor	Flywheel (>10krpm)	Lithium-ion (general)	Lead Acid battery
System Round-Trip Efficiency (RTE) [%]	92	86	86	72
Response Time [sec]	0.016	0.25	1	1
Cycles at 80% Depth of Discharge	1 000 000	200 000	3500	900
Life [Years]	16	>20	10	2.6
Cell voltage [V]	2.3 to 3	-	3.6	2
Specific energy (Wh/kg)	5	10 – 50	120 – 240	35 - 40
Specific power (W/kg)	Up to 10 000	1000–5000	1000–3000	180
Cost per kWh [$/kW]	74480	11520	469	549
Cost per kW [$/kWh]	930	2880	1876	2194
Self-discharge % in 30 days	5-40	1-2 (per hour)	<5	3-20
Charge temperature [°C]	–40 to 65	-	0 to 45	−35 to 45
Discharge temperature [°C]	–40 to 65	-	–20 to 60	−35 to 45

As seen from Table 1, the Supercapacitors have the highest specific power, cycles, and also the lowest cost per kW, which makes them ideal devices for fast energy delivery and absorption, especially in transportation. In this sense, they, as well as Flywheel, are power storing devices in the sense that they can deliver and absorb very high amounts of energy

in a very short time, and this way differ very much from other energy storing devices like batteries.

Thus, as the use of Supercapacitors is increasing, the Department of Electrical Power Engineering Mechatronics in TalTech needs such kind of laboratory equipment for educational purposes, as the Supercapacitors have quite different behaviour from battery, as discussed in greater detail in chapter 2.1.

A search of existing laboratory test benches did not yield results, despite the fact that almost every manufacturer of power electronics has some products on their list related to supercapacitors. The main finished products are intended for micro grids, but most of the products are offered as custom made.

The equipment used in the articles are also of local origin, as the main focus is on control systems or the development of converters better matching with the specific properties of Supercapacitors.

There are some Supercapacitors Development Boards commercially available from Texas Instrument [2] and Analog Devices [3]. They intend for the development of consumer energy backup systems using their SC control chips (bq33100 and DC1937B correspondingly), including 4-5 capacitors, half-bridge DC-DC converter. The power of them is some tenth of watts and they have software to control and monitor Supercapacitors. In terms of suitability, however, they are more for the development of consumer electronics and do not provide practical experience of using high power components and modules as they are in use in electric vehicles or microgrids.

So, in this situation, it is quite reasonable to build a test bench if most of the key components of rather expensive power electronic components and modules as listed in Appendix 4 (BOM) already exist.

1.1 Task Description

The Department of Electrical Power Engineering Mechatronics of TalTech needs a test bench for laboratories when teaching Supercapacitor properties and energy storing devices using them. In The Department of Electrical Power Engineering Mechatronics, the Simulation Platform for Power Electronic Systems PLECS [4] for modelling,

designing and simulation, is widely used. As a hardware complement to PLECS, there are several RT-Boxes in use, which enables both real-time hardware-in-the-loop (HIL) testing and the rapid control prototyping [5].

So, the main task is to develop a model in PLECS software for the control system using visual blocks provided by software and rebuild the existing bench so that it could be driven from the RT-Box that has the created PLECS model in it.

The expected parameters of the converter in the bench are:

- The voltage on DC bus up to 300 V, which average rectified amplitude of 230V AC powerline;
- Power, up to 3 kW, which is maximum allowable power from one phase on powerline;
- Capable of charge Supercapacitors up to 144 V.

The existing components are:

- 3 serially connected supercapacitors for energy storing, each with rated capacity 165F, voltage 48 V (144 V in total), absolute maximum voltage 52 V, ESR 6.3 mΩ, current 100A and absolute maximum current 1900 A [6];
- Bench with power source with inductive filter up to a 3,6 kW, which is maximum power to one phase AC powerline;
- Synchronous-Buck converter with isolated drivers of IGBT transistors and isolated sensors for output current and voltage.

2 Overview of Technology

2.1 Supercapacitors

An Electric Double Layer Capacitor (EDLC) or simply Supercapacitor (SC) also called Ultracapacitor, is defined as a device using induced ions between an electronic conductor such as activated carbon and an ionic conductor like as organic or aqueous electrolyte. [7]

The construction of Supercapacitor, compared to other main types of capacitors, shown on Figure 1. The electrodes of porous material are connected with metal current collecting electrodes, separated by separator and filled with electrolyte.

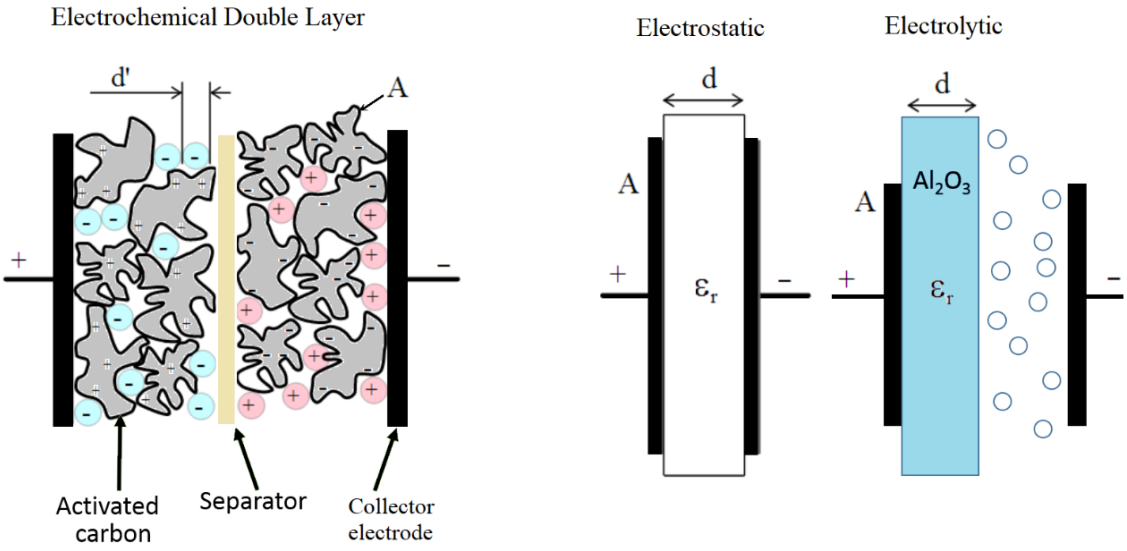

Figure 1 Supercapacitor construction.

The capacitor's capacitance, as general, is determined by formula (1), where it comes that to increase the capacitance, the area *A* of electrodes should be increased and distance *d* between them decreased.

$$C = \varepsilon_r \varepsilon_0 \cdot \frac{A}{\mathrm{d}} \tag{1}$$

Decreasing the distance, like it is done in electrolytic capacitors by very thin oxide, on the other hand reduces rated voltage, increasing the area of electrodes increases dimensions.

In Supercapacitor, active carbon is used as electrodes, which is porous material having effective surface area 1000 to 2300 m^2/g. The effective charge separation distances *d'* in Supercapacitor, is also very small, on the order of 10 Å (1 nm) or less. [8]

The Supercapacitors voltage ratings depend on the electrolyte used. In case of using organic electrolytes, the voltage ratings up to 3.0 V per cell, typically 2.7 V and 3.0 V, whereas with aqueous electrolytes the voltage rating less than 1.23 V per cell, typically 0.9 V. [8]

The energy stored into capacitor is described by formula (2):

$$E_C = \frac{C \cdot V_C^2}{2} \tag{2}$$

Thus, the capacitor can be considered as empty, if the voltage has dropped by half, then the residual energy is 25 %. This is, compared with battery, illustrated in Figure 2.

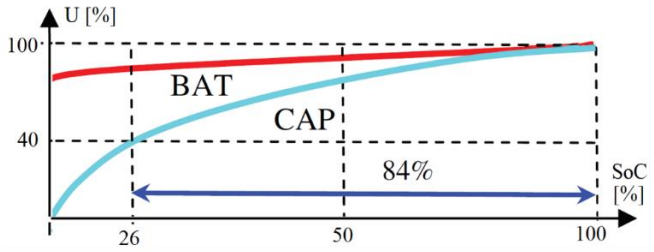

Figure 2 Typical voltage vs. state of charge dependence for batteries/capacitors. [9]

The formula (2) determines the supercapacitor charge-discharge profiles shown on Figure 3 [10].

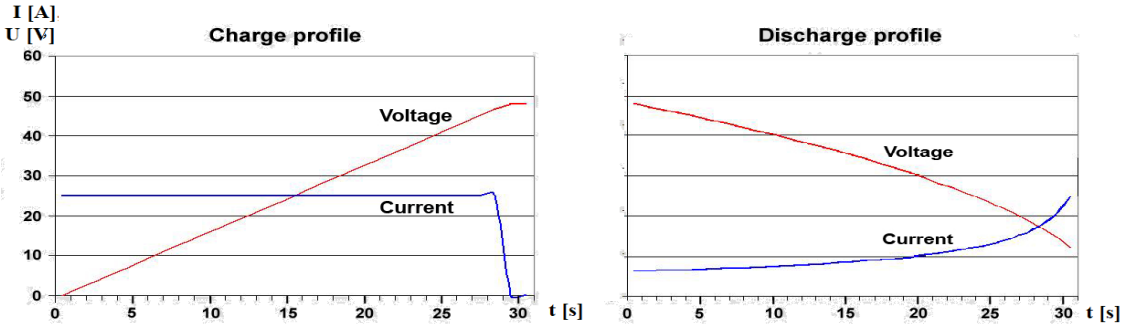

Figure 3 Supercapacitors charge-discharge profiles.

The discharge profile mainly makes special demands on the converter, as at constant power the voltage is dropping as the current is rising.

Supercapacitors, by nature, do not determine the upper voltage, but at some point a voltage breakdown occurs. Thus, the Supercapacitors have very strictly limited voltage, which is most commonly 2.7 V per cell. According to [11], the lifetime doubles if working voltage lowered from 2.7 V to 2.5 V per cell.

Theoretically, the Supercapacitors are symmetrical as shown on Figure 1, and thus don't have polarity, but for example, to protect the steel case of individual shells, and etc., the polarity is clearly specified. Thus, no immediate catastrophic failure occurs to a SC if polarity is reversed, but, for long life, it is strongly recommended that the polarity of the SC has been monitored.

Such a low voltage needs series connection of cells to obtain higher voltages, which causes need for balancing, usually these units are already integrated by the manufacturer.

The charge-discharge cycles of Supercapacitors are virtually unlimited (measured in millions) compared to batteries (a couple of thousands), making them perfect short time energy storing devices.

By time, a supercapacitor ESR increases 100% at the end of their lifecycle. This means an additional SC voltage drop, as the current consumption also increases during the discharge process, according to Figure 3. The increased ESR also means additional heat dissipation in SCs. [11]

The energy storage efficiency mainly depends on ESR and usually over 98%, but can be reduced significantly when used in high currents, but should be still above 90%.

The supercapacitor reaction time is much slower than an electrolytic capacitor and usually around 1 second to charge a capacitor 63.2% of full charge or discharge to 36.8% of full charge. [12]. So, they are not suitable for high current ripple as they can overheat.

2.2 Converter Topologies

For energy conversion, in energy storage systems, bidirectional DC-DC (BDC) converters are used, which depending on applications, can be isolated or non-isolated.

The most used basic non-isolated types are Synchronous Buck/Boost or simply Half-bridge (Figure 4a) and cascaded Buck-Boost or simply Full-bridge, often also called H-bridge Converter (Figure 4b) [13].

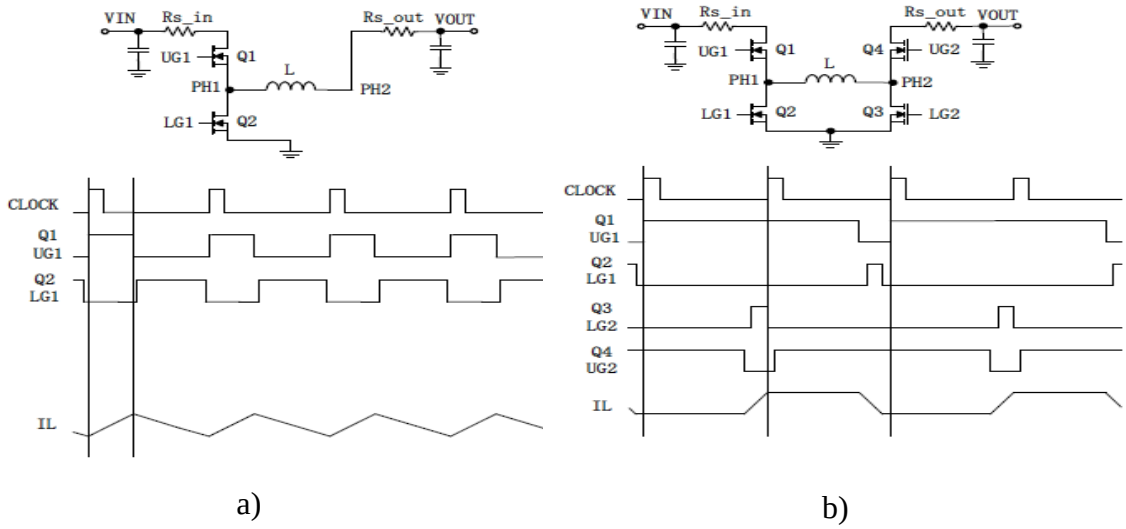

a) b)

Figure 4 Half-bridge (a) and full-bridge (b) converter circuit and operation waveforms. [13]

Half-bridge converter needs less switches and is also simpler to control and the working principle is also better to understand, which is important as the bench is for teaching purposes. The Half-Bridge converter has strictly defined high and low voltage sides. Full-Bridge converters do not have this disadvantage and can raise or lower voltage in either direction.

There are also other base converter topologies having bi-directional versions shown on Figure 5 and discussed in context of electric bus in [14] in and in detail, including voltage and current stresses of components, in [15].

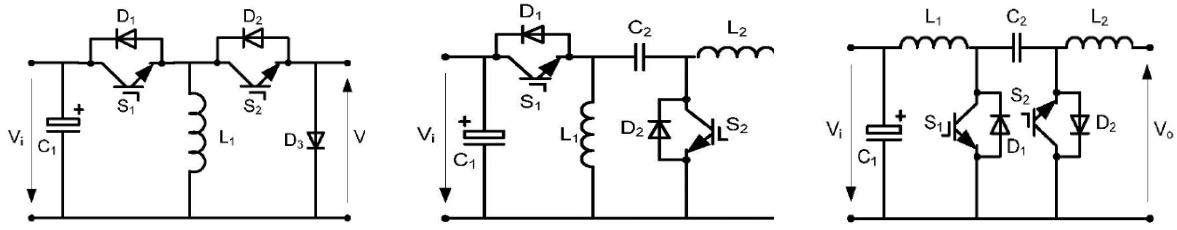

a) b) c)

Figure 5 Bi-directional versions of base converter topologies: (a) Buck-Boost converter, (b) ČUK and (c) LUO/SEPIC converter. [14]

The Buck-Boost (Figure 5a) converter input and output voltages are opposite and thus voltage stress on switches are $U_{in}+U_{out}$ which significantly lowers the voltages that can be used in high power systems.

The LUO/SEPIC converter (Figure 5b) works as LUO mode in charging operation and SEPIC mode in discharging operation, and the ČUK converters (Figure 5c) benefits are that it is symmetrical in both directions and the current is continuous. [14]

Both the ČUK and the LUO/SEPIC converters drawbacks on needs of large non-polar transfer capacitors which are expensive according to [14], but they also need two power inductors.

As a rule of thumb, a non-ideal non-isolated transformerless voltage rising (Boost) converter has the capability to raise a voltage up to 3-4 times. Thus the difference between low voltage side (Buck mode) and high voltage side (Boost mode), cannot differ more than 3 times, considering efficiency. So, in systems without a transformer, the rated voltage value of the stored device must be high enough, the ratio of DC bus and energy stored device would be below that.

There are also interesting topologies like [16] that exist, trying to overcome voltage rising limits, but they are not suitable for learning purposes as they are not intuitive to understand. Detailed description and overview of isolated bidirectional converters in [17]. They are characterized as at least double of switches and magnetic components. Keeping in mind learning purposes, simplicity and easy understanding of the working principles is preferred.

In commercial applications, multiphase converters shown in Figure 6, are commonly used.

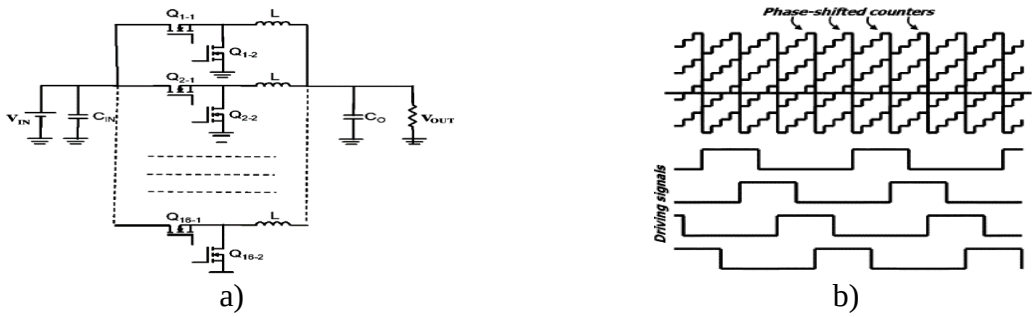

Figure 6 Multiphase dc-dc converter (a) topology and (b) corresponding waveforms number of phases is 4.

Multiphase topology allows to increase the power of the converter and in the same time reduce pulsations both in output as well as in input (Figure 7). [18].

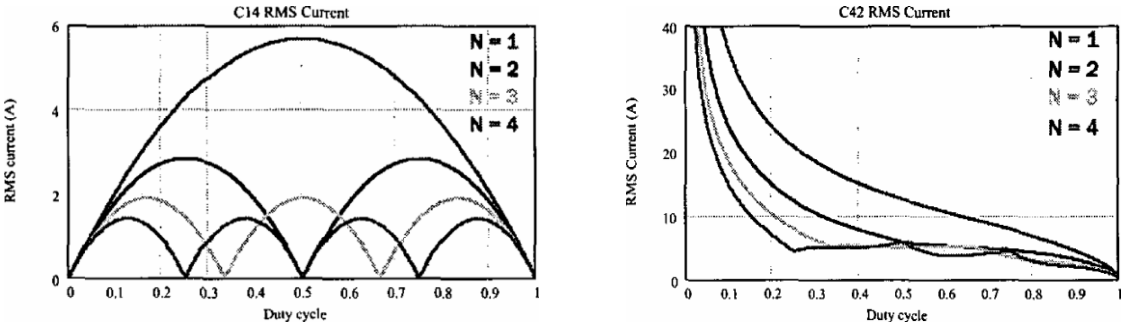

a) b)

Figure 7 The RMS current in Buck converter (a) input capacitor C_{IN} and (b) output capacitor C_{OUT} as a function of the number of phases and the duty cycle. [18]

Although multiphase converters are widely used in commercial applications, they can in principle be considered as several single converters connected in parallel and synchronously controlled. Thus, in the meaning of learning converters basics, a simple one phase converter is enough.

2.3 Control Systems of Converters

Primary energy sources in DC grids like batteries and especially Fuel Cells, have limited currents and current changing speed. This is also for batteries, considering their safe work and long lifespan. As mentioned in 2.1, the Supercapacitors on other hand, can handle high charging and discharging currents, but the current still has limitations, but they are very sensitive to voltage and if overvoltage occurs on the Supercapacitor cell, it most probably will be destroyed. Thus protection against overvoltage is very important to be used.

The most common power stage, used as a bidirectional converter, is half-bridge as the simplest and robust.

The most used control system in power electronics is the Proportional-Integral (PI) controller. Typically, bi-directional converters, used for Supercapacitors and batteries, have double closed loop controller where first, inner loop, controls the average current using PI algorithm ([18], [19], [20], [21], [22], [23]) and then, the outer loop, controls the voltage (Figure 8).

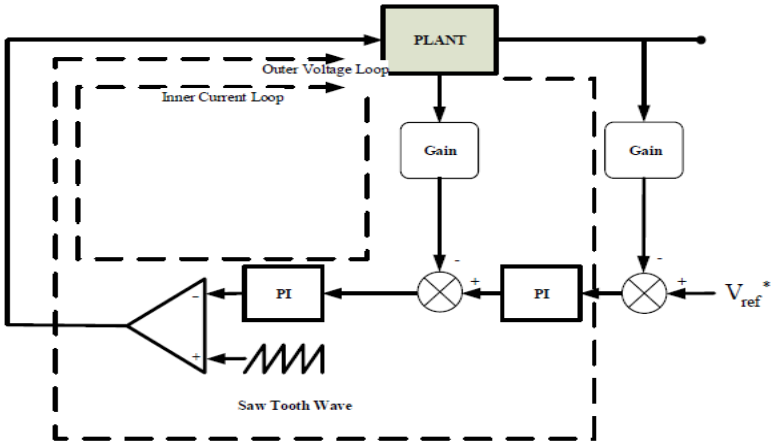

Figure 8 Closed loop control diagram commonly used in Bidirectional Converter. [20]

The current flow is controlled and limited by the inner loop according to the storage device used in the system. The direction of the energy flow is then regulated by monitoring the State-of-Charge (SoC) of the energy storage device and the DC bus.

In [24], is proposed a control for battery charge-discharge using PI and anti-Windup by current for inner loop, and by both in/out voltages, for outer loop (Figure 9). More detailed descriptions of different anti-windup schemes described in [25], [26].

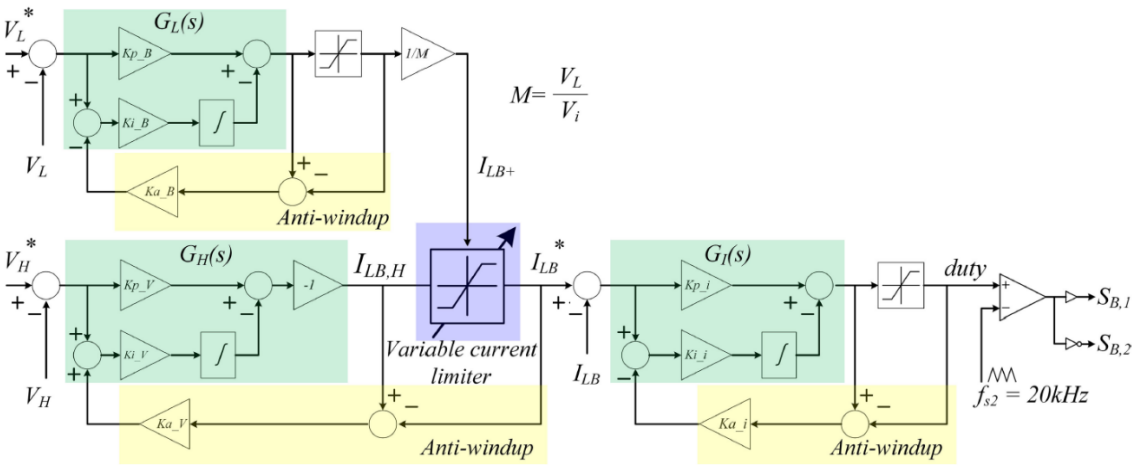

Figure 9 Control block diagram of the proposed battery charger in [24].

So, the most promising topology to use for the laboratory bench is a half-bridge power stage and the control system of a double PI controller of an average current controller as in the inner control loop and DC bus voltages as an outer control loop.

3 Power Electronics Design

In The Department of Electrical Power Engineering Mechatronics, the Simulation Platform for Power Electronic Systems PLECS [4] for modelling, designing and simulation, is widely used. As a hardware complement to PLECS, there are several RT-Boxes in use, which enables both real-time hardware-in-the-loop (HIL) testing and the rapid control prototyping [5].

3.1 Design Selection

Bidirectional converter can be seen as Buck converter in one direction and Boost converter in another. Boosting and lowering directions are explicitly specified in the half-bridge converter shown on Figure 10 in as Boost converter.

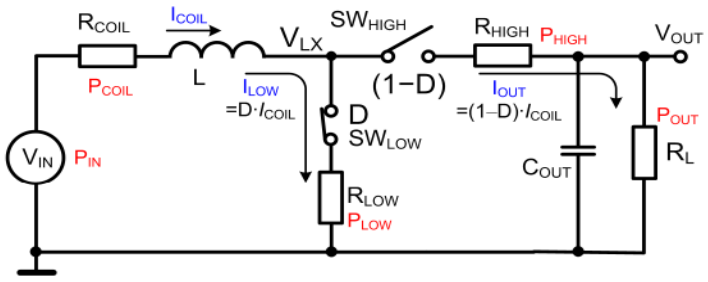

Figure 10 Boost Converter schematic with parasitic components. [27]

When in a Buck converter the voltage difference between input and output is mainly the matter of total efficiency, then the non-isolated Boosting converter (without transformer) has noticeable limitations. According to [27] the Boost converter (Figure 10) has limitation described by formula (3) and relation between input-output voltage and duty cycle (D) by (4):

$$D_{crit} = 1 - \sqrt{\frac{R_{coil}+R_{LOW}}{R_L}} \tag{3}$$

$$D = 1 - \frac{V_{IN}}{V_{OUT}} \tag{4}$$

So, there are certain points where the output voltage of the boost converter achieves its maximum and additional increase of duty cycle decreases the output voltage. Thus, the normal proportional relationship between D and V_{OUT} becomes reversed (illustrated on Figure 11).

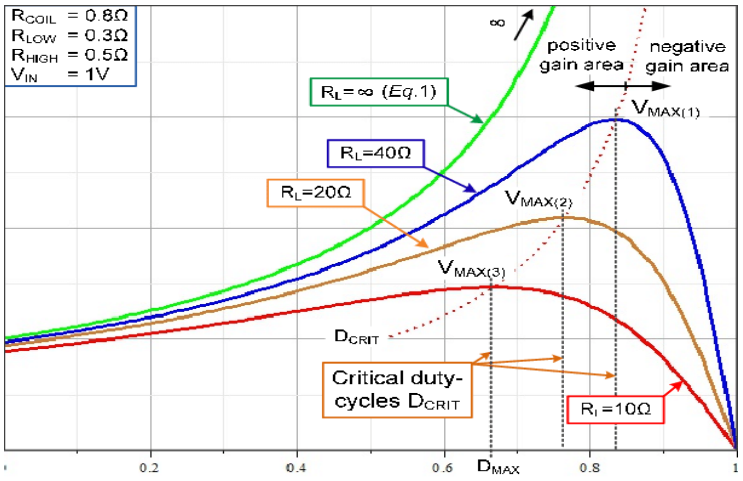

Figure 11 Output voltage dependency of boost converter depending on the duty cycle. [27]

The Supercapacitor on another hand, as discussed in chapter 2, have very strictly limited voltage absolute maximum 2.7 V per cell and typical modules 12 V, 24 V and 48 V (although higher voltage modules also exist), and capacitor energy described by formula (2).

The DC lines are typically around 400 V, thus the half-bridge converter is very suitable as the voltage of existing capacitors are up to 144 V which is always less than a typical DC line and desired DC voltage of test bench.

3.2 Half-bridge Converter Calculations

Defining the system parameters as SC charge-discharge current 20 A, U_{DC_bus}=300 V, U_{SC_min}=72 V, U_{SC_max} 144 V, taking inductor current ripple 10 % of SC charge-discharge current, which is Δi=2 A and considering audible noise of converter, the switching frequency taken 20 kHz.

As half-bridge can be seen as Back or Boost converter depending from current direction, the inductance and ripple current dependency can be described by formulas (5)(6) [28]:

$$I_{ripple\_Buck} = \frac{V_{in}-V_{out}}{L} \cdot t_{on}$$

$$I_{ripple\_Boost} = \frac{V_{in}}{L} \cdot t_{on} \quad (5)$$

Where t_{on} is switch on time:

$$t_{on} = D \cdot T = D \cdot \frac{1}{f_s} = \frac{D}{f_s} \tag{6}$$

And duty cycle D for both mode types calculated:

$$D_{Buck} = \frac{V_{out}}{V_{in}}$$

$$D_{Boost} = 1 - \frac{V_{in}}{V_{out}} \tag{7}$$

The needed inductance is the maximum of inductance needed for Buck and Boost and when putting all formulas (5)(6)(7) together, replacing corresponding V_{in} and V_{out} voltages by V_{low} and V_{high}, the resulting formula (8) for both Buck and Boost modes is the same. The inductance is the highest when low side voltage is 144V and calculated as:

$$L = \frac{1}{f_s \cdot I_{ripple}} \cdot \frac{(V_{high} - V_{low})\, V_{low}}{V_{high}} = \frac{1}{20\ kHz \cdot 2\ A} \cdot \frac{(300\ V - 72\ V)\ 72\ V}{300\ V} = 1872\ \mu H \tag{8}$$

Since the inductor is 12.6 mH or 7 times larger, but with a tape core, it was expedient to reduce the switching frequency. Taken the switching frequency 5 kHz from formula (8) the new ripple is where current ripple and inductance reverse related, the current ripple will be also 7 times less, 0.286 A. The actual current ripple, show on Figure 12, measured, when converter works in Boost mode at 5 kHz, at average current 1,77 A, is 370 mA.

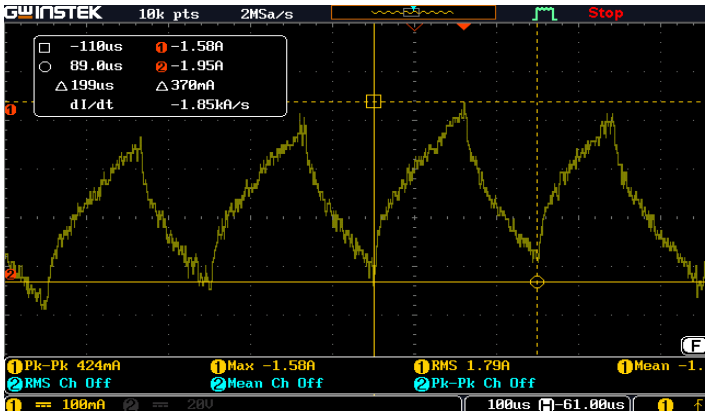

Figure 12 Measured current ripple of used inductor.

3.3 Existing Hardware

The existing bench contained several components, there were two inverters, several power supplies, and fuses, inductors, capacitors and three serially connected Supercapacitor modules. The SC modules are described in greater detail in 3.4.

- Bench with several installed components Figure 13.

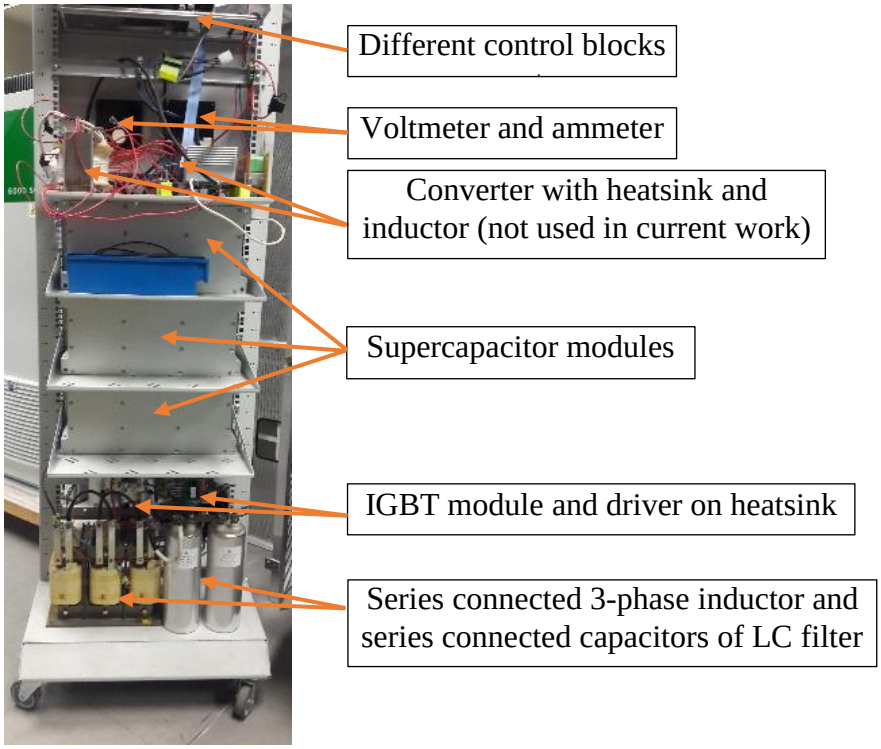

Figure 13 Initial test bench at the beginning of the work (from up): converter with heatsink, control blocs and inductor; three Supercapacitor modules; second converter with driver module mounted on heatsink; and power LC filter.

- IGBT Power Module (Half-bridge) BSM 75 GB 120 DN2 with collector current 105 A and collector-emitter voltage 1200 V [29] mounted on heatsink together with driver module 2SD315AI-33 for Half-bridge IGBTs up to 3.3 kV isolation, peak current of gate drive I_{out} ±18 A, output power for both channels 6 W, supply voltage 15 V and maximum supply current 470 mA [30].

- Two voltage sensors with 3-way isolated (input, output and power) amplifiers MCR-C-UI-UI-450-DCI with configurable I/O, for the electrical isolation of analogue signals, with cut-off frequency (3 dB) 450 Hz, Supply voltage range

18 V to 30 V, current consumption < 30 mA (without load), maximum transmission error ≤ 0.1 % and step response (10-90 %) 0.8 ms. [31]

- Power supply MPS3-230/24C from AC 230 V as input and DC 24 V up to 3 A as an output. [32]
- Capacitor PPM416.47.0012 by DUCATI Energia SpA with 200 µF ±10%, nominal voltage U_n=450 V noted on it.
- 3-phase inductor R-3-03K3-AN with inductance 1 mH, 100 Hz and 6 kV noted on it.

Components added to bench:

- Closed Loop Hall effect current sensor LA 55-P for DC, AC pulse currents' measurements with galvanic isolation of nominal rating up to 50 A, conversion ratio 1:1000, no load power consumption 10 mA from ±12 V to ±15 V. [33]
- 3-phase bridge rectifier S3PDB180N16 with average forward current 139 A and reverse voltage 1800 V, peak current 1800 A width duration less than 10 ms. [34]
- Capacitor 947C731K801CDMS for inverter applications with 730 µF, rated voltage V_r=800 V, I_{rms}=58 A, ESR=3.5 mΩ and ESL=65 mΩ. [35]
- RT-Box adapter board, schematic and layout shown in Appendix 2.
- Inductor with two windings (Figure 14), each of them measured 12.6 mH and saturation current using only one winding measured 20 A. The saturation current measurement is described in more detail in next chapter 3.3.1.

Figure 14 Inductor that was used in the converter.

3.3.1 Measuring Inductors Saturation Current

To measure the inductor saturation current the testing scheme shown on Figure 15 was used according to suggestion on [36].

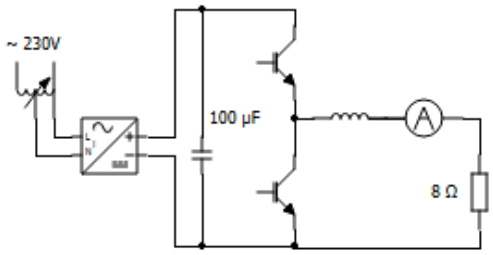

Figure 15 Inductor saturation current measurement scheme.

The converter was permanently set to a switching with duty cycle D = 0.5, and the output voltage of the autotransformer was increased smoothly until the oscilloscope display showed a significant extension of the peaks in the form of a current flowing through the choke. The waveforms are shown on Figure 16.

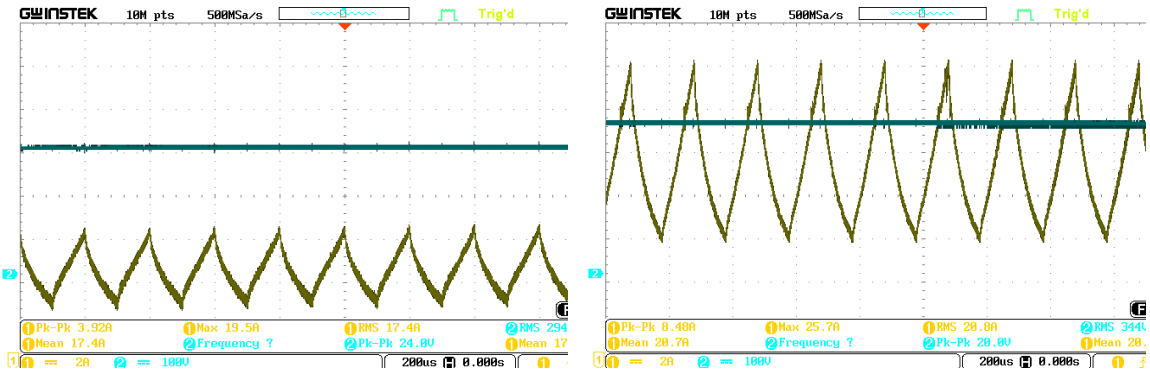

a) b)

Figure 16 Measuring inductors saturation current by waveforms distortion: non-distorted normal waveform (a) distorted when inductor is become saturated (b).

As can be seen on Figure 16b, the current triangular waveform is significantly extended, compared to normal one on Figure 16a and also the peak-to-peak current ripple increases significantly. So, the value of the saturation current of the choke lies below 20 A.

3.4 Supercapacitor Modules

The used Supercapacitor modules in test bench are BMOD0165 P048 BXX from Maxwell Technologies, are intended for use in Hybrid vehicles, Rail, Heavy industrial equipment and UPS systems and have outputs for Temperature and Overvoltage, Active Cell Balancing built inside, with dimensions are 418×194×179 mm (L×W×H). [6]

a) b)

Figure 17 Supercapacitor module c [6] (a) and series connection of three modules in test bench (b).

The Supercapacitor modules, shown on Figure 17a, are connected in series with short and thick copper bars Figure 17b.

3.4.1 Protection logic

The protection logic cables for overvoltage and thermal monitoring, shown on Figure 18, are not yet connected.

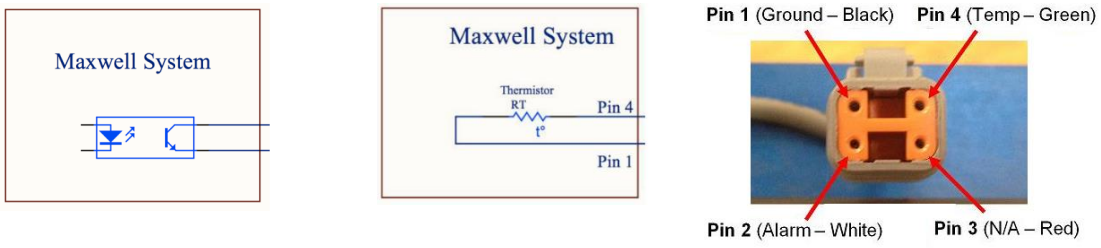

a) b) c)

Figure 18 Protection logic in SC module: (a) the overvoltage system, (b) 10 kΩ thermistor schematic and (c) cable connection pinouts. [37]

3.4.2 Active Cell Balancing

Maxwell Technologies uses Active Cell Balancing built inside modules Figure 19. [38]

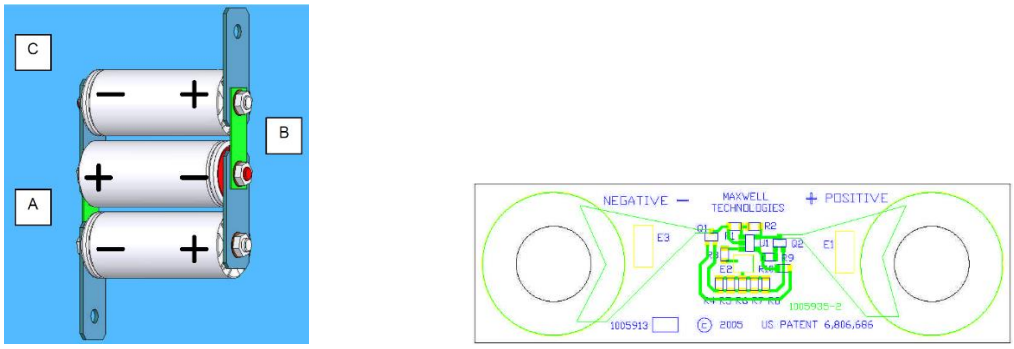

a) b)

Figure 19 Maxwell Technologies Active Cell Balancing (a) module connections and (b) board layout.

The balance boards are connected to the midpoint of two cells (board B, with A-C central point) and if there are some misbalance, the Balance Board starts to drive current to the midpoint so that both cells have the same voltage. Overview of balancing module parameters in Table 2.

Table 2 Balance Board Parameters

Accuracy	± 0.02 V
Voltage range	1.2 – 2.9 V
Humidity, 25 ºC	95%
Humidity, 40 ºC	80%
Temperature range	-40 to 85 ºC
Leakage current when balanced	50 mA
Balance current	max 300 mA
Busbar current rating	200 A_{RMS}

3.4.3 Current

Although the absolute maximum current of the SC module is 1900 A, the continuous current is depending from ESR and ambient temperature by formula (9):

$$\Delta T = I_{RMS}^2 \cdot ESR \cdot R_{CA} \quad (9)$$

Where R_{CA}=0.40 ºC/W is the thermal resistance of all cells cases to ambient and ΔT is temperature difference of all cells to ambient. [6]

3.5 Sensors of the Test Bench

The bench was completely unwired and all power connections were made using at least 6 mm^2 wires. All unnecessary components and modules were removed. The existing suitable modules and components were verified for working and searched for datasheets.

For the RT-Box using, there was additionally added RT-Box connection board having connectors for connecting RT-Box and fibre optic connector for the switch drivers. For this purpose, 1.5 m long fibre cables are made.

3.5.1 Voltage Sensors

They were configured to have up to 20 V in input and output up to 10 V, which were the maximum possible values. Both voltage dividers for voltage sensors were calculated to having 500 V at the input and 20 V at the output, thus dividing factor 1:25. The voltage divider with corresponding thermal and voltage stress on each resistor, shown on Figure 20a.

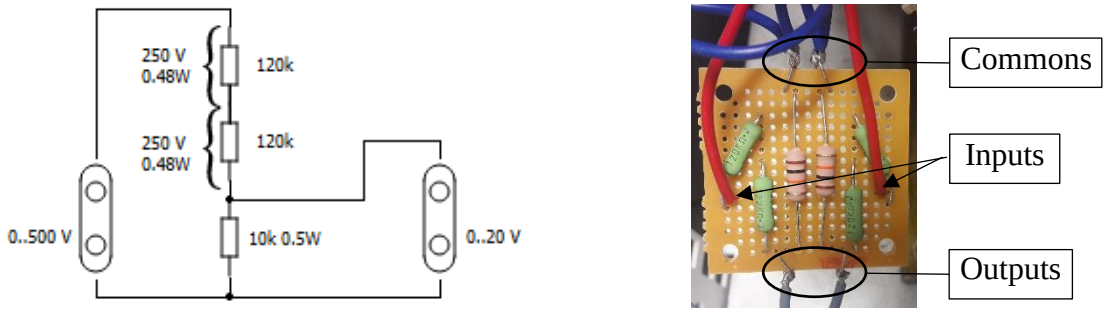

a) b)

Figure 20 Voltage divider (a) schematic of voltage divider with power dissipation and voltages of high side resistors and (b) the both voltage dividers are made as a hanging assembly on a breadboard.

Based on the power dissipated on the voltage divider and to minimize voltage stress of resistors (shown on left of resistors on Figure 20a), the high side of voltage divider was formed of two serially connected 120 kΩ 2 W resistors and 10 kΩ 0.5 W for the low side was enough. Both voltage dividers were mounted on common 5×5 cm breadboard (Figure 20b).

The voltage divider module was mounted directly to the voltage sensors input screw terminals to be as close as possible to voltage sensors to prevent interferences.

The voltage sensors with divider boards were placed at the bottom of the bench near the power section to keep high voltage cables short. The outputs of the voltage sensors were brought to the RT-Box adapter board with a shielded 4-core cable.

3.5.2 Current Sensor

The current sensor has current output with conversion ratio 1:1000 means 50 A of current going through the sensor gives 50 mA at the sensors output and 5 V voltage drop on 100 Ω resistor, the value selected from allowed range on datasheet [33].

Hall-effect sensors are sensitive to magnetic fields and it is important to keep in mind to mount far enough from any of these big inductors used in the converters.

3.5.3 Calibrating Sensors

Before starting a tuning controller with real hardware, the current and voltage sensors need calibration. For this reason, to into the model were added temporary gain elements tuneable online. In this way the calculated scaling factors of the analogue inputs adjusted accordingly the readings of measurement equipment.

3.6 Modified Test Bench

The rebuilt test bench shown on Figure 21.

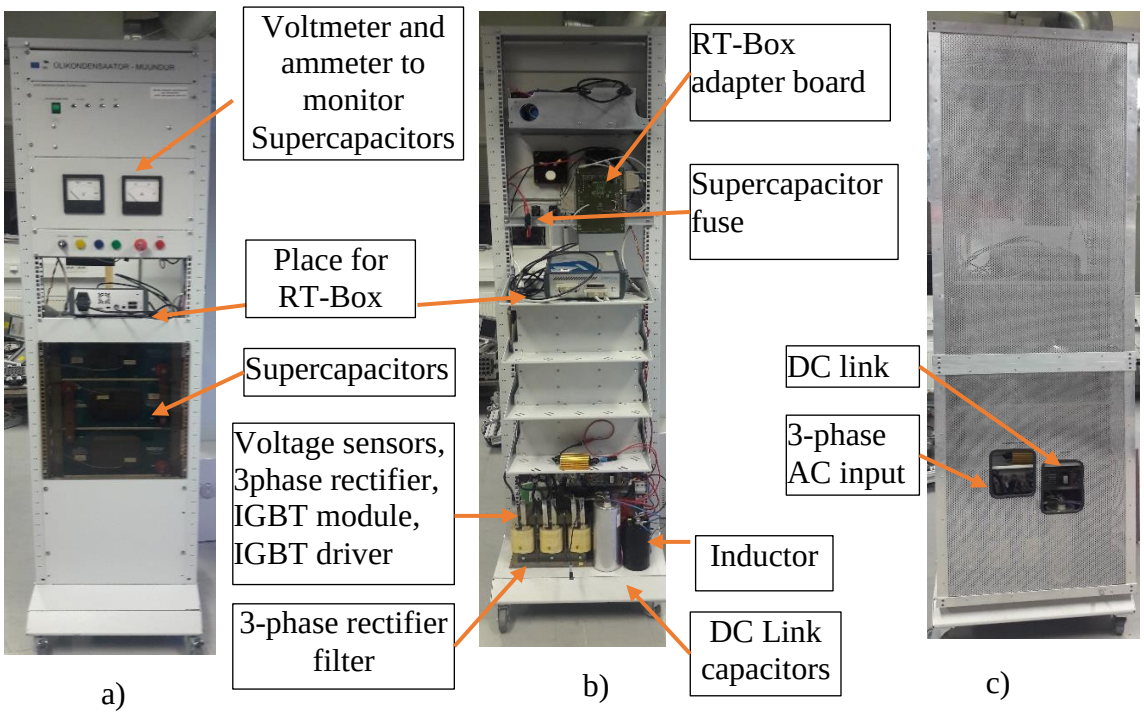

Figure 21 Rebuilt test bench from front (a), insight (b) and covered backside (c).

3.7 Setting up RT-Box Controlling System

The test bench setup is shown on Figure 22.

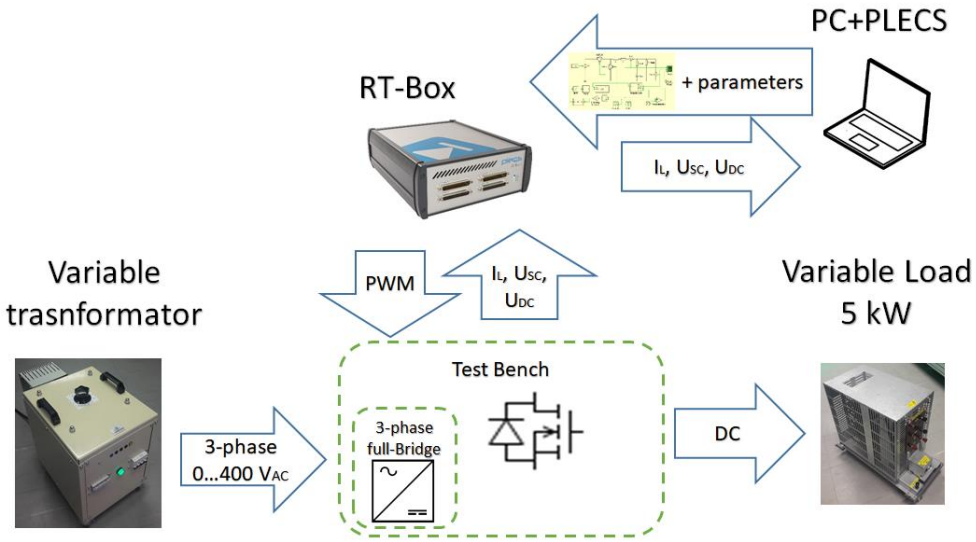

Figure 22 System setup and workflow of verification on the testing bench.

To prepare an upload of the control model from PLECS into the RT-Box, the RT-Box has to be connected to the computer running the PLECS via Ethernet cable. The simulation model is to be divided into a control part and a power plant part, as shown on Figure 23.

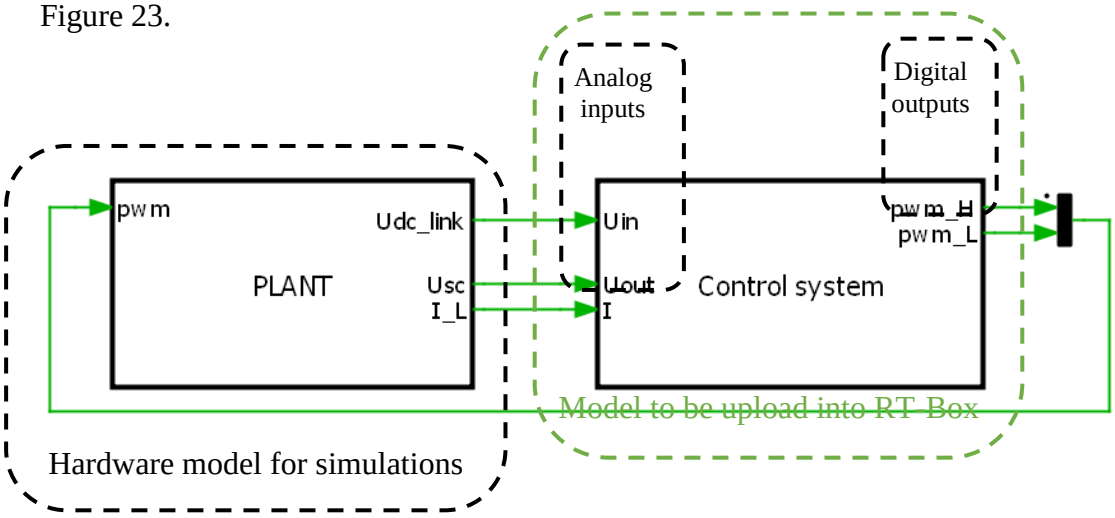

Figure 23 Full model divided into Control System to be uploaded and power plant used for further simulations.

The Control System model also has real RT-Box input and outputs connected to the converter via RT-Box Adapter board to drive switches and read actual sensor values.

When setting up the system, it is advisable to synchronize data acquiring and PWM switching to reduce interferences on sensor readings.

To proceed with tuning, several nodes like switches and constants, added to the list of online configurable parameters, so they are adjustable when the model is running.

4 Control

The development process is the following. First, a model is created in PLECS. Its performance is evaluated in a simulation and, finally, tested on real hardware of the bench, using an RT-Box as a controller.

Controller's main principle is double loop control (Figure 24). Inner loop controls the current when the outer loop controls the DC bus.

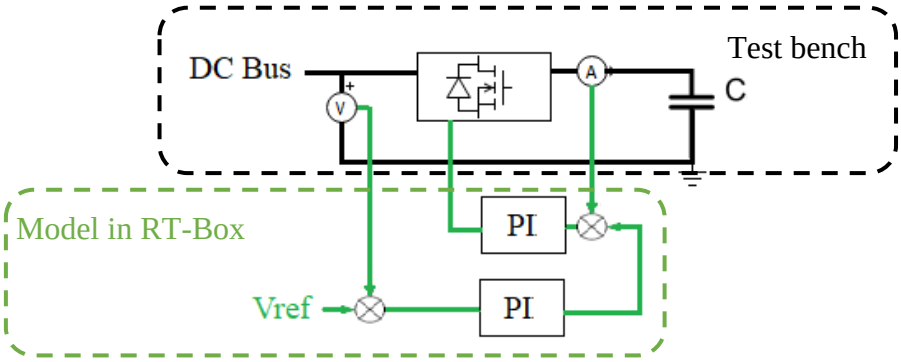

Figure 24 Double loop feedback diagram, inner loop by current outer by DC bus voltage and dividing between the system into real hardware and PLECS model loaded into RT-Box.

4.1 Current Controller

The inner loop controls the average current in both directions – charge and discharge of SC. The simplest control system is PI.

4.1.1 Current Loop Controller Model

From the control system fast response and good stability demanded at the same time. The best way to test the controller response is with impulses, when the system is also more prone to instabilities, in worst case even oscillations.

For tuning the PI controller, the common Ziegler-Nichols method has been used. Additionally, upper and lower saturation limits have been added to the integral part of the PI controller.

The current change of tuned model to the control pulse shown on Figure 25.

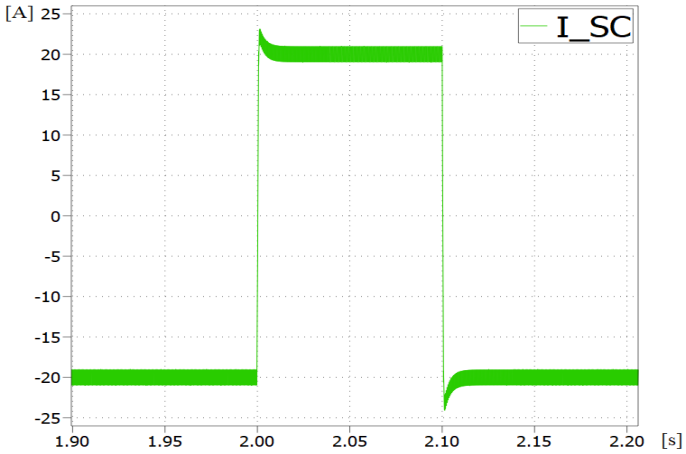

Figure 25 Change of current to control pulse.

There are overshoots at both transition times, but they are of an acceptable size and stabilizes within 10 ms.

4.1.2 Current Loop Controller on Real Hardware

Testing with real convert started with reduced current 5 A to keep inductor far away from saturation. To test reaction of current control, the square wave signal was given as the current reference from -5 A to 5 A. Result of the measured current of inductor and voltage of DC link shown on Figure 26.

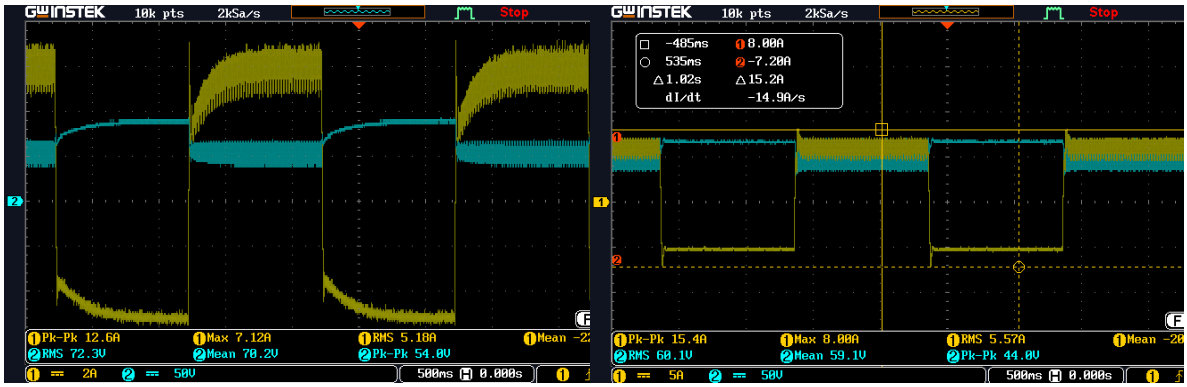

a) b)

Figure 26 Testing current control reaction with square wave: (a) preliminary result and (b) after tuning controllers PI parameters.

As can be seen from Figure 26b the reaction is faster but has some overshoots, which are tolerable, but must be kept in mind as with increase of average current, these overshoot amplitudes also must remain below inductor saturation current level.

4.2 DC Bus Voltage Controller

The simplest control method to control the outer loop by voltage is still the PI regulator.

Controlling of DC link and State-of-Charge of supercapacitor and other parameters, for example, if the vehicle is still, it probably starts moving and needs additional energy and thus capacitor better to be charged maximally, are considered to be out of this work as they are application specific.

The base principle is simple. There are upper and lower limits set for DC link Figure 27.

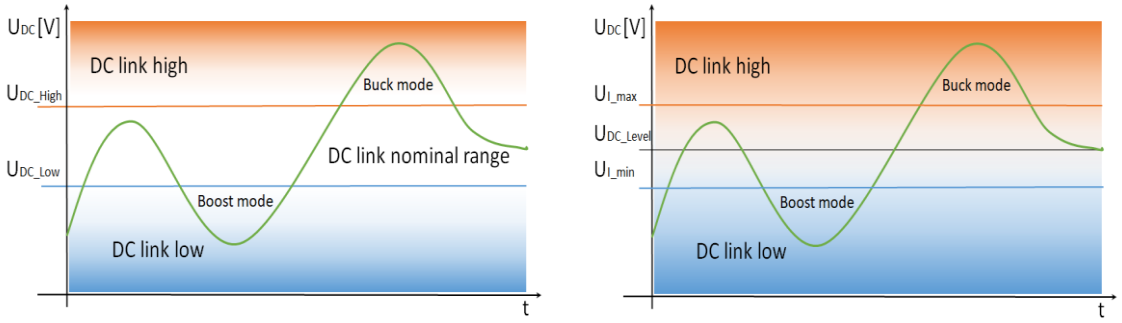

a) b)

Figure 27 DC link voltage levels (a) typical handling logic and (b) currently used simplified handling logic.

For learning purposes, the logic should be as simple and understandable as possible. Thus, for the voltage control, the nominal voltage level is set and above that level is charging region where inductor current is positive, the converter work as Buck converter and converter tries to bring the DC link voltage down to the nominal voltage level, at the same time charges Supercapacitor. Below that level is the discharging region where the current is negative, the converter works as a Boost converter trying to hold up the nominal DC link voltage level.

4.2.1 Controller Model

The model of full controller (Appendix 3) based on the double PI controller method discussed in chapter 4 and some nodes were added. The main unit involved directly in the controlling process is Control Logic (Figure 28).

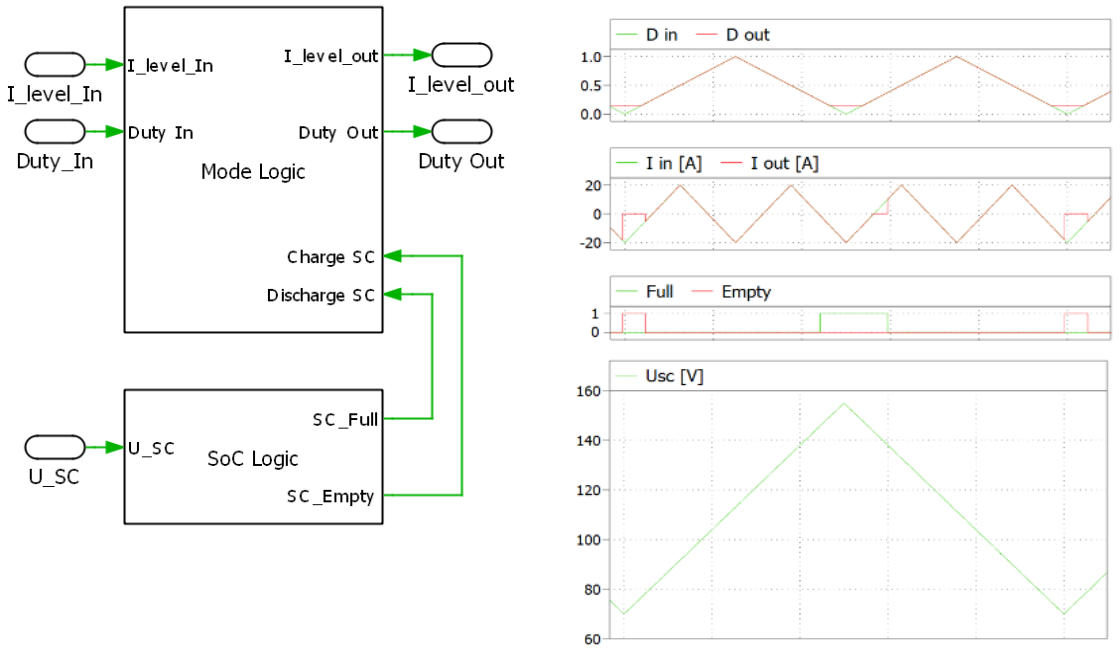

a) b)

Figure 28 Logic module blocs: (a) mode control Buck/Boost (upper) and Supercapacitor state of charge (lower) and (b) acting diagrams.

The functions are divided into two parts. The SoC Logic monitors for Supercapacitor voltage as discussed in chapter 2 and signals “empty” when voltage goes below the set voltage level where the capacitor is considered empty, and when voltage rises above threshold value, the “empty state” is removed. The same logic goes for the “full” state shown (Figure 28b).

The “Mode Logic” (Figure 28a) monitors for the average current set by the PI controller of DC Link and limits the current to be set for the converter by the PI controller according to the difference of the measured voltage.

4.3 Protection Logic for Supercapacitor

System components also need protection, in addition to the average current control loop which is limited to 20A. There can also be transient peak currents. The main principle is to stop the switching of the converter.

The overcurrent protection is set to 35 A, and if this happens, the converter switches off and needs to be started manually when malfunction is handled.

The Super capacitor is very sensitive to overvoltage, so switching is turned off when the SC voltage reaches 144 V or drops below 72 V. To avoid instabilities, a delay and hysteresis of 10 % was added, so the switching will be restored when the SC voltage is far enough from the limits or if the controller mode is changing i.e., from charging the SC to discharging and vice versa.

Result of the protection system simulation with specifically designed current waveform, shown on Figure 29.

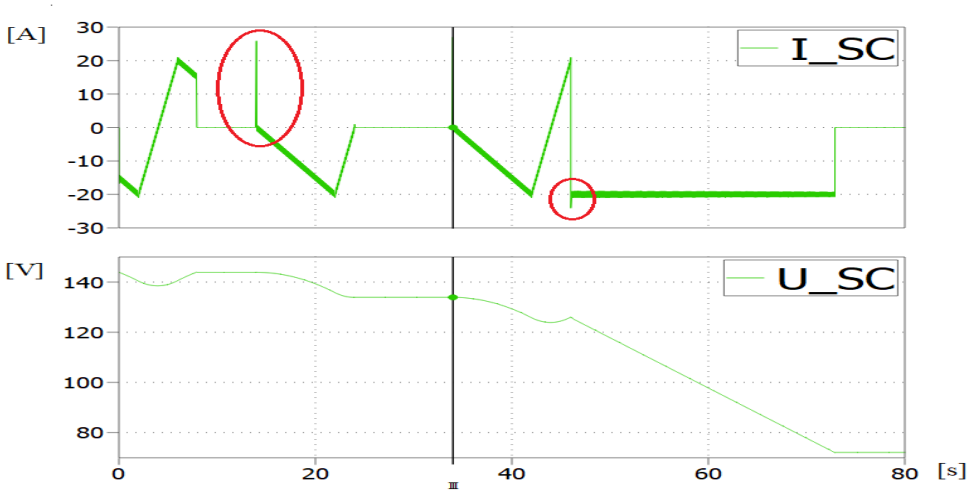

Figure 29 Simulations of the SC charge and discharge limit protection.

4.3.1 Protection Logic for Switches (transistors)

Before testing with real hardware, an additional safety unit was added to the model's Control System part shown on Figure 30.

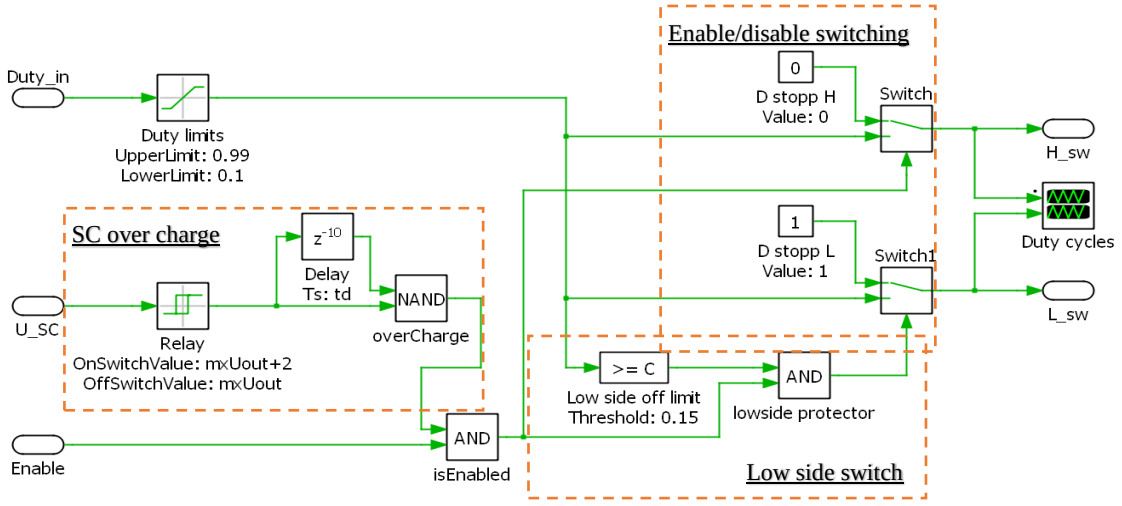

Figure 30 Safety module to protect supercapacitors and low-side transistors.

The main functions needed to be realised are:

1) Section “Enable/disable switching”. Enable and disable switching of the converter;

2) Section “Low side switch”. Protection of the low side switch from overcurrent caused by long relative time when switch is open and energy captured into inductor. Taking into account limitations described in chapter 3.1 it is reasonable to set the lower limit of the duty cycle between 0.1 and 0.3 and when duty cycle is les, for example when starting of charging of completely empty supercapacitor, then the low side switch should be kept switched off letting converter to act as simple Buck;

3) Section “SC over charge”. Protection the supercapacitor from overcharge. If the voltage of the supercapacitor should ever reach the set limit U_{out_cutoff}, this means something is wrong and the converter remains turned off until this malfunction has been eliminated. This section contains delay to ensure that overcharge limitations weren't occasional disturbance.

5 Testing the Bench

For testing the converter the DC link voltage level was 200 V, the working current 10 A with overcurrent stop 15 A. And load 64 Ω if not mentioned otherwise.

5.1 Testing Charging of the Supercapacitor

To test the full charge of the supercapacitor, the DC bus voltage with the autotransformer was set to about 230 V, as the set DC link voltage level was 200 V. A strong ripple of the DC link voltage can be seen on Figure 31, as only one phase was used for power supply. When the voltage of the supercapacitor reaches a predetermined level of 130V, the charging is switched off and when the charging current falls close to zero, a strong ripple of the DC bus is also lowered notably.

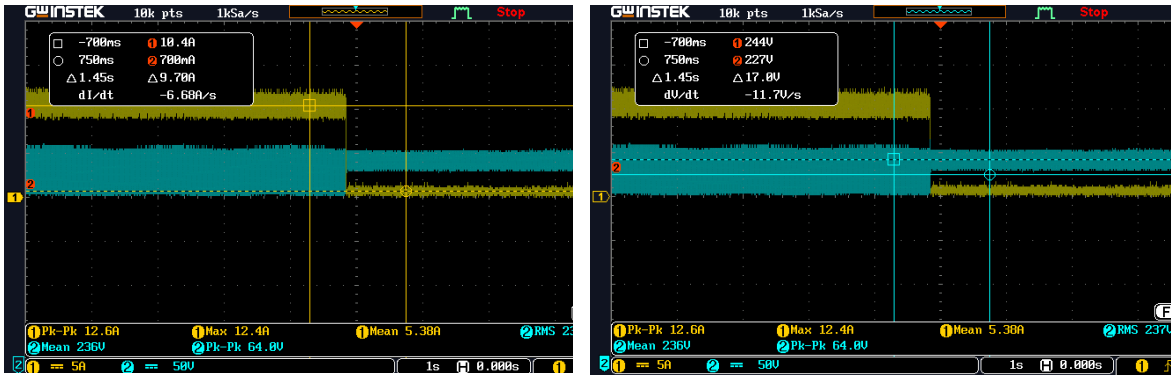

a) b)

Figure 31 Oscillograms of inductor (a) current and (b) DC link voltage (b) at the moment the supercapacitor is full and the converter stops the charging.

As seen on Figure 31, the stopping of charging is fast and there are no overshoots notable. The hysteresis levels set for fully charged were set 130 V and 117 V.

5.2 DC Bus Voltage Maintenance Test

For test to see how converter keeps DC link voltage and switch between charging and discharging, the load was changed to 32 Ω. Rd response to changing of input voltage of DC link around 200 V by changing the output of the autotransformer by turning the corresponding knob. Result is shown on Figure 32.

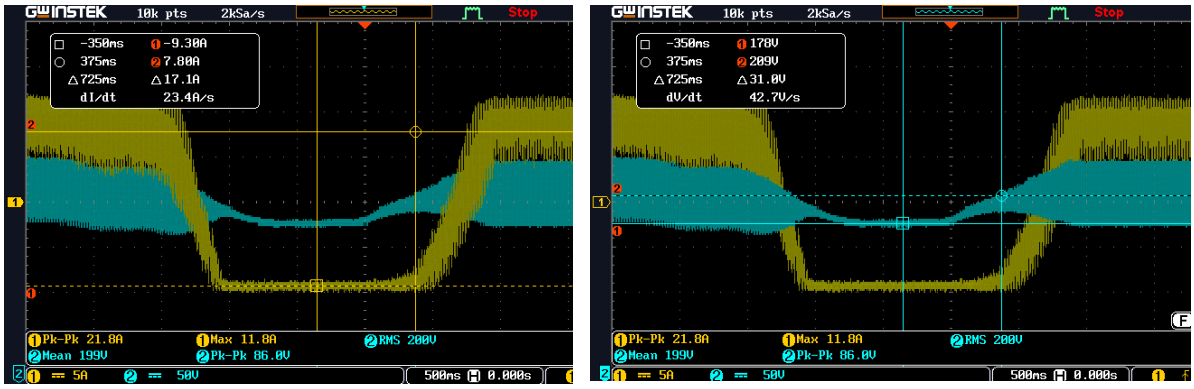

a) b)

Figure 32 Oscillograms of (a) inductor current and (b) DC link voltage when DC link voltage is fluctuating above and below set DC link value 200 V.

There are also strong voltage ripple DC link voltage can be seen on Figure 32, it keeps the voltage at 178 V which 11% less and 209 V which is 4.5 % over, so in 10% round.

5.3 Load Change Test

Testing the reaction of the converter for the load change, especially to disconnect and reconnect the load, is important as the bench is meant for teaching, and thus it is a highly possible case. The response for the disconnecting and reconnecting the 32 Ω. load when converter is working Boost mode e.g., rising voltage of DC link set to 120 V, is shown on Figure 33.

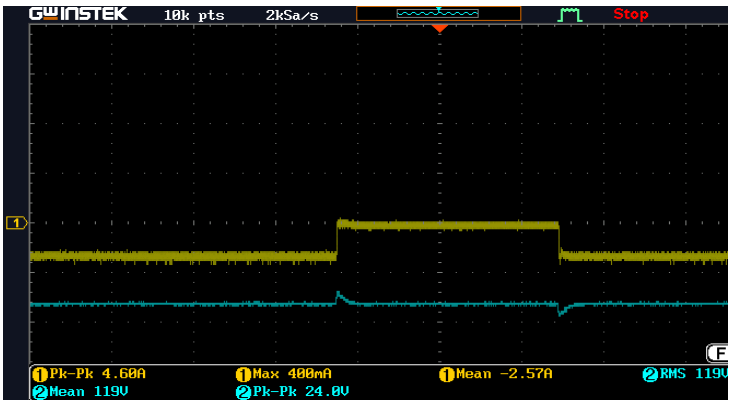

Figure 33 Reaction of converter to disconnection of 64 Ω load.

There are, visible some overshoots around 10 % and no current shoots are notable. The relatively low voltage overshoots are as expected as the bidirectional converter inherently transfers energy to balance voltages on both sides to match the current duty factor.

5.4 Efficiency Test

The efficiency of the converter was not the main goal, but it is a mandatory part of every converter measurement. The most problematic is the Boost mode of operation of the converter, so the measurements were made for discharging of capacitor only.

The process is as follows. The supercapacitor charged until full, e.g., when voltage reaches previously set value 130 V, and then turning off the input, the converter starts to keep the pre-set DC link voltage and simultaneously were measured DC link voltage and, inductor current and supercapacitor voltage was taken every time the supercapacitor voltage drops 5V. The measurements were made with a DC link loaded with 32 Ω and voltage set to 160 V, as the maximum raised voltage was 188 V. The current in DC the link is calculated from DC link voltage and load. Results of measured coil current, SC and DC ling voltages and the calculated parameters of efficiency and voltage rising factor are shown on Figure 34.

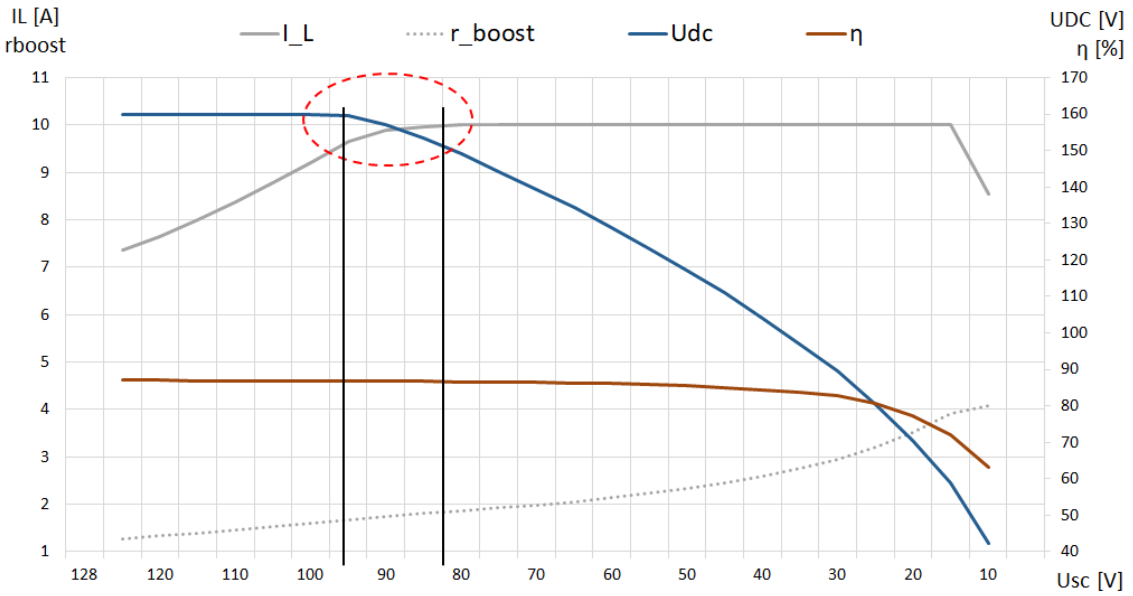

Figure 34 Efficiency and Boost ratio of converter, DC link voltage and coil current depending on voltage on supercapacitor.

As expected, at some point converter is not able to keep up the DC link voltage from certain point U_{SC}=95 V where, r_{boost}= 1.68. But there is also the range indicated by a circle in Figure 34, where the DC link voltage drops, but the choke current has not yet reached the maximum allowable value. This is probably can be adjusted by increasing gain, but according to formula (2), supercapacitors have already given up 57% of their initial

energy. From U_{SC} = 80 V, the conversion is already limited due to the maximum current I_L = 10 A.

The overall effectiveness 87 % is as expected. It is not high in modern standard, but very much acceptable, especially taking into account used inductor in such a kind that are most likely designed to work as filters at 100 Hz frequency range.

5.4.1 Supercapacitor Resistance Test

A used supercapacitor has internal resistance ESR= 6.3 mΩ each [6], in addition to the ESR, the internal resistances of the cables (together approximately 5 m) and connections and the ammeter, are added. The voltage sensors are connected as far as possible from Supercapacitors - directly to the switch and inductor.

The measurement procedure is as follows. The supercapacitor is charged with a constant current to a certain voltage and the direction of the current is reversed - discharge begins. After the system has stabilized, the flow direction is changed again. In both current direction changes, the voltage and current changes are measured, from which the resistance of the supercapacitor circuit is calculated.

The oscillograms of the obtained signals are on Figure 35 and the numerical data are summarized in Table 3.

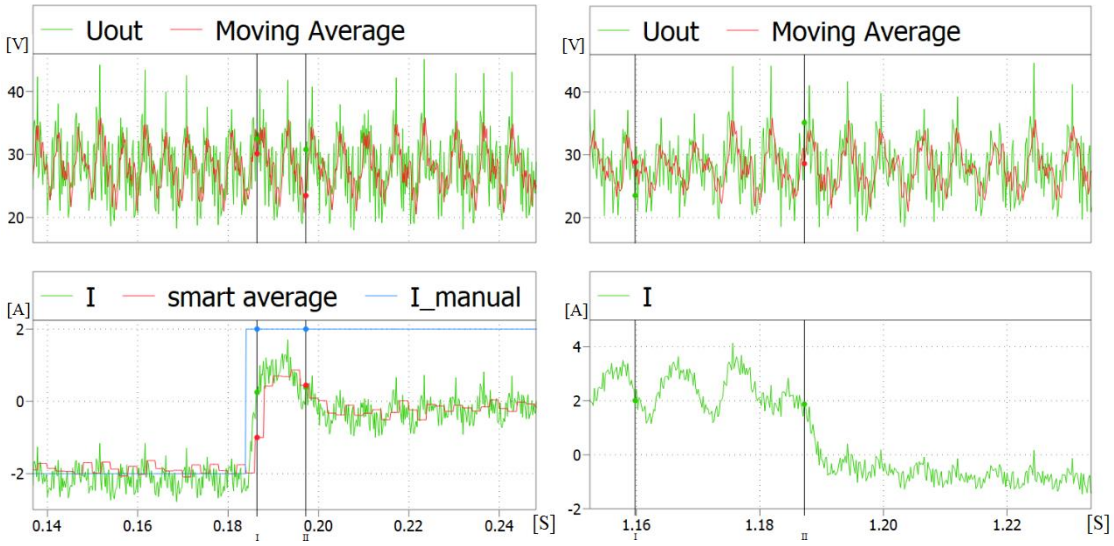

Figure 35 Supercapacitor ESR measurement current and voltage slope diagrams.

As seen on Figure 35, the change of voltage on the SC is very small and is buried in the noise and disturbance. So the only way to get any information is to average a reasonable number of measurements by setting cursors on graphs. The results of mean values before and after the transition processes are gathered into Table 3.

Table 3 ESR Measurements and calculations

Change direction	Starting state		Ending state		ΔU	ΔI	ESR
	U_{mean}	I_{mean}	U_{mean}	I_{mean}			
Charge to Discharge	27.91 V	2.35 A	28.47 V	-0.47 A	0.56 V	2.83 A	0.20 Ω
Discharge to Charge	27.74 V	-2.14 A	28.27 V	0.71 A	0.53 V	2.85 A	0.19 Ω

The calculated ESR around 0.2 Ω seems quite adequate, but it was not possible to verify it due to the absence of equipment capable of measuring low resistances. It is also possible that the ESR of three capacitor modules serially connected, has been raised from 18.9 mΩ to 37.8 mΩ, as discussed in chapter 2.1.

6 Summary

The basic construction and general principles of control of the simplest supercapacitor converter are considered in the work, and a physical test bench is realized. Therefore, the work can also be considered as a step-by-step construction of a two-way converter, from the basic calculations to the tuning of the converter, can also be taken as a part in the teaching process.

The principles of current distribution on a shared DC link and the charging and discharging of a supercapacitor have also been implemented. General principles, problematic nodes and elements, and circuit breakers in control are described.

The practical part of this work shows the problems and nuances of a real inverter, which in computer simulations cannot be taken into account at first glance, such as high noise in sensors and switching pulses when switching various units in the control module, and even when connecting a powerful autotransformer to the mains. So, in this work can also be found helpful tips for learners making their first steps working with Supercapacitors and power converters building and modelling controllers.

It was confirmed that one of the most critical elements of the converter power section is the inductor, which essentially determines the parameters of the entire converter and the failures of which are likely to result in failure of the active elements. It is also not only a large element in terms of dimensions and weight, but also a costly element, the acquisition of which in its finished form is rather problematic.

6.1 Conclusions

The current configuration is not very optimal. The switches, switch driver, capacitors and rectifier have high voltage capability and to realize their full potential DC bus should have around 800 V, but used supercapacitors one other hand have low voltage, only 144 V when fully charged, but can give enormous amount of current (absolute maximum of 1900 A). The non-isolated half-bridge converter is simple, robust and relatively low cost having a low number of components, but cannot raise voltage as much as needed.

Thus, in case of commercial usage, the better solution would be to put more capacitors with less capacitance in series to rise voltage, up to 750 V is allowed.

Another option is lower the DC link voltage and use a multiphase converter with high current (and low voltage capable) switches to increase current and also lower current ripple.

6.2 Future Work

It follows from this work that the existing choke does not allow to realize the full potential of other existing elements of the converter. Therefore, as a continuation of the work, it is planned to calculate a choke with a core of up to 100 A iron scrap, to order the necessary ring cores and to prepare the necessary choke yourself.

It is also necessary to find a solution for the development of additional security of the trend, especially with regard to the fast-acting short-circuit protection of the DC link, as this is a teaching tool and misuse is more likely.

References

[1] K. Mongird, V. Fotedar, V. Viswanathan, V. Koritarov, P. Balducci, B. Hadjerioua and J. Alam, “Energy Storage Technology and Cost Characterization Report,” HydroWIRES, 07 2019. [Online]. Available: https://energystorage.pnnl.gov/pdf/PNNL-28866.pdf. [Accessed 05 2021].

[2] J. Li, “Backup Power Solution Using Supercap with TPS61030 for Data Concentrator Circuit,” Texas Instruments Incorporated, [Online]. Available: https://www.ti.com/tool/BQ33100EVM-001. [Accessed 05 2021].

[3] “LTC3350EUHF Demo Board,” Analog Devices, Inc, [Online]. Available: https://www.analog.com/en/design-center/evaluation-hardware-and-software/evaluation-boards-kits/dc1937b.html.

[4] “The Simulation Platform for Power Electronic Systems,” Plexim GmbH, [Online]. Available: https://www.plexim.com/products/plecs. [Accessed 5 11 2020].

[5] “RT Box 1,” Plexim GmbH, [Online]. Available: https://www.plexim.com/products/rt_box/rt_box_1. [Accessed 5 11 2020].

[6] “48V MODULES,” Maxwell Technologies INC, [Online]. Available: https://www.maxwell.com/images/documents/hq_48v_ds10162013.pdf. [Accessed 5 11 2020].

[7] M. Endo, T. Takeda, Y. J. Kim, K. Koshiba and K. Ishii, “High Power Electric Double Layer Capacitor (EDLC's); from Operating Principle to Pore Size Control in Advanced Activated Carbons,” *Carbon letters,* vol. 1, pp. 117-128, 01 01 2001.

[8] J. Miller, J. Miller and R. Smith, “Maxwell Technologies White Paper: Ultracapacitor Assisted Electric Drives for Transportation,” Maxwell Technologies, Inc., [Online]. Available: https://www.maxwell.com/images/documents/whitepaper_electricdrives.pdf. [Accessed 05 2021].

[9] C. Klumpner, G. Asher and G. Z. Chen, “Selecting the power electronic interface for a supercapattery based energy storage system,” in *2009 IEEE Bucharest PowerTech,* Bucharest, Romania, 2009.

[10] “BU-209: How does a Supercapacitor Work?,” 13 05 2021. [Online]. Available: https://batteryuniversity.com/learn/article/whats_the_role_of_the_supercapacitor.

[11] P. Kreczanik, P. Venet, A. Hijazi and G. Clerc, “Study of Supercapacitor Aging and Lifetime Estimation According to Voltage, Temperature, and RMS Current,” *IEEE Transactions on Industrial Electronics ,* vol. 61, no. 9, pp. 4895 - 4902, 2014.

[12] “Design Considerations for Ultracapacitors. Maxwell Technologies White Paper: Design in Guide,” Maxwell Technologies, Inc., [Online]. Available: www.maxwell.com. [Accessed 2021].

[13] D. Zhan, “Design Considerations for a Bidirectional DC/DC Converter,” Renesas Electronics Corp, 2018. [Online]. Available: https://sub.allaboutcircuits.com/white-papers/design-considerations-bidirectional-dc-dc-converters.pdf. [Accessed 27 10 2020].

[14] K. Zhiguo, Z. Chunbo, Y. Shiyan and C. Shukang, “Study of Bidirectional DC-DC Converter for Power Management in Electric Bus with Supercapacitors,” in *IEEE Vehicle Power and Propulsion Conference*, 2006.

[15] R. Schupbach and J. Balda, “Comparing DC-DC converters for power management in hybrid electric vehicles,” in *IEEE International Electric Machines and Drives Conference*, Madison, WI, USA, 2003.

[16] W. Jiang and B. Fahimi, “Phase-Shift Controlled Multilevel Bidirectional DC/DC Converter: A Novel Solution to Battery Charge Equalization in Fuel Cell Vehicle,” in *IEEE Vehicle Power and Propulsion Conference*, Arlington, 2007.

[17] B. Zhao, Q. Song, W. Liu and Y. Sun, “Overview of Dual-Active-Bridge Isolated Bidirectional DC–DC Converter for High-Frequency-Link Power-Conversion System,” *IEEE Transactions on Power Electronics,* vol. 29, no. 8, pp. 4091-4106, 8 11 2013.

[18] M. Gerber, J. A. Ferreira, I. W. Hofsajer and N. Seliger, “Interleaving optimization in synchronous rectified DC/DC converters,” in *IEEE 35th Annual Power Electronics Specialists Conference (IEEE Cat. No.04CH37551)*, Aachen, 2004.

[19] B. Li, C. Xu, C. Li and Z. Guan, “Working principle analysis and control algorithm for bidirectional DC/DC converter,” *Journal of Power Technologies,* vol. 97, pp. 327-335, 9 2017.

[20] K. S. Mukesh, B. S. Subhendu and M. Srikanta, “Closed loop control of a new non-isolated quadratic boost converter,” in *2017 International Conference on Communication and Signal Processing (ICCSP)*, Chennai, India, 2017.

[21] W. Wu, Y. Chen, A. Luo, L. Zhou, X. Zhou, L. Yang, Y. Dong and J. M. Guerrero, “A Virtual Inertia Control Strategy for DC Microgrids Analogized With Virtual Synchronous Machines,” *IEEE Transactions on Industrial Electronics,* vol. 64, no. 7, pp. 6005 - 6016, 2017.

[22] B. Amrouche, T. Cherif, M. Ghanes and K. Iffouzar, “A passivity-based controller for coordination of converters in a fuel cell system used in hybrid electric vehicle propelled by two seven phase induction motor,” *International Journal of Hydrogen Energy,* vol. 42, no. 42, pp. 26362-26376, 2017.

[23] J. Mehran, S. Qobad, G. Mehrdad and B. Hassan, “Control of a super-capacitor energy storage system to mimic inertia and transient response improvement of a direct current micro-grid,” *Journal of Energy Storage,* vol. 32, p. 101788, 12 2020.

[24] J. Park and S. Choi, “Design and Control of a Bidirectional Resonant DC–DC Converter for Automotive Engine/Battery Hybrid Power Generators,” *IEEE Transactions on Power Electronics,* vol. 29, no. 7, pp. 3748 - 3757, 16 9 2013.

[25] G. Anirban and J. Vinod, “Anti-windup Schemes for Proportional Integral and Proportional Resonant Controller,” in *NATIONAL POWER ELECTRONIC CONFERENCE*, 2010.

[26] C. Bohn and D. Atherton, “An analysis package comparing PID anti-windup strategies,” *IEEE Control Systems Magazine,* vol. 15, no. 2, pp. 34 - 40, 4 1995.

[27] M. Vratislav, “Dynamic duty-cycle limitation of the boost DC/DC converter allowing maximal output power operations,” in *2016 International Conference on Applied Electronics (AE)*, Pilsen, Czech Republic, 2016.

[28] M. Zehendner and M. Ulmann, “Power Stage Topology Reference Guide,” Texas Instruments Incorporated, [Online]. Available: https://www.ti.com/lit/pdf/slyu036. [Accessed 2020].

[29] 05 05 2021. [Online]. Available: https://www.mouser.ee/datasheet/2/196/infineon_eupcs02842-1-1735611.pdf.

[30] “2SD315AI-33 Data Sheet,” Power Integrations, [Online]. Available: https://www.power.com/file-download/download/public/1064. [Accessed 05 05 2021].

[31] “Signal conditioner - MCR-C-UI-UI-450-DCI - 2810887,” PHOENIX CONTACT GmbH & Co. KG, 05 05 2021. [Online]. Available: https://www.phoenixcontact.com/.

[32] “Detailed information for: MPS3-230/24C,” ABB, [Online]. Available: https://new.abb.com/products/64209396/power-supply-mps3-230-24-coated-power-supply-mps3-230-24-coated.

[33] “LA 55-P,” LEM International SA, [Online]. Available: http://www.lem.com/sites/default/files/products_datasheets/la_55-p_e.pdf. [Accessed 05 05 2021].

[34] Sirectifier Electronics Technology Corporation, [Online]. Available: http://www.sirectifier.net/uploadfile/fj_pdf/20161019193065246524.pdf. [Accessed 05 05 2021].

[35] “Type 947C Polypropylene, DC Link Capacitors,” [Online]. Available: https://www.cde.com/resources/catalogs/947C.pdf. [Accessed 05 05 2021].

[36] “How to Avoid Inductor Saturation in your Power Supply Design,” [Online]. Available: https://www.monolithicpower.com/en/how-to-avoid-inductor-saturation-in-your-power-supply-design. [Accessed 29 05 2021].

[37] “User Manual. Ultracapacitor Energy Storage Modules Powered by DuraBlue™ Technology,” Maxwell Technologies, [Online]. Available: www.maxwell.com. [Accessed 05 2021].

[38] “BOOSTCAP Integration Kit. Applicable for the following ultracapacitor cells,” Maxwell Technologies, Inc., [Online]. Available: http://www.maxwell.com. [Accessed 2021].

[39] O. Garcia, P. Zumel, A. de Castro and A. Cobos, “Automotive DC-DC bidirectional converter made with many interleaved buck stages,” *IEEE Transactions on Power Electronics,* vol. 21, no. 3, pp. 578 - 586, 8 5 2006.

[40] A.Rassõlkin and V.Vodovozov, “TEST BENCH WITH SUPERCAPACITOR STORAGE TO STUDY PROPULSION DRIVES,” pp. 65-70, 2013.

Appendix 1 – Non-exclusive licence for reproduction and publication of a graduation thesis[1]

I Gabriel Villers

1. Grant Tallinn University of Technology free licence (non-exclusive licence) for my thesis
   "RT-Box Controlled Laboratory Test Bench for Teaching Super Capacitor Properties" , supervised by Indrek Roasto
   1.1. to be reproduced for the purposes of preservation and electronic publication of the graduation thesis, incl. to be entered in the digital collection of the library of Tallinn University of Technology until expiry of the term of copyright;
   1.2. to be published via the web of Tallinn University of Technology, incl. to be entered in the digital collection of the library of Tallinn University of Technology until expiry of the term of copyright.
2. I am aware that the author also retains the rights specified in clause 1 of the non-exclusive licence.
3. I confirm that granting the non-exclusive licence does not infringe other persons' intellectual property rights, the rights arising from the Personal Data Protection Act or rights arising from other legislation.

10.05.2021

1 The non-exclusive licence is not valid during the validity of access restriction indicated in the student's application for restriction on access to the graduation thesis that has been signed by the school's dean, except in case of the university's right to reproduce the thesis for preservation purposes only. If a graduation thesis is based on the joint creative activity of two or more persons and the co-author(s) has/have not granted, by the set deadline, the student defending his/her graduation thesis consent to reproduce and publish the graduation thesis in compliance with clauses 1.1 and 1.2 of the non-exclusive licence, the non-exclusive license shall not be valid for the period.

Appendix 2 – RT-Box Adapter Board

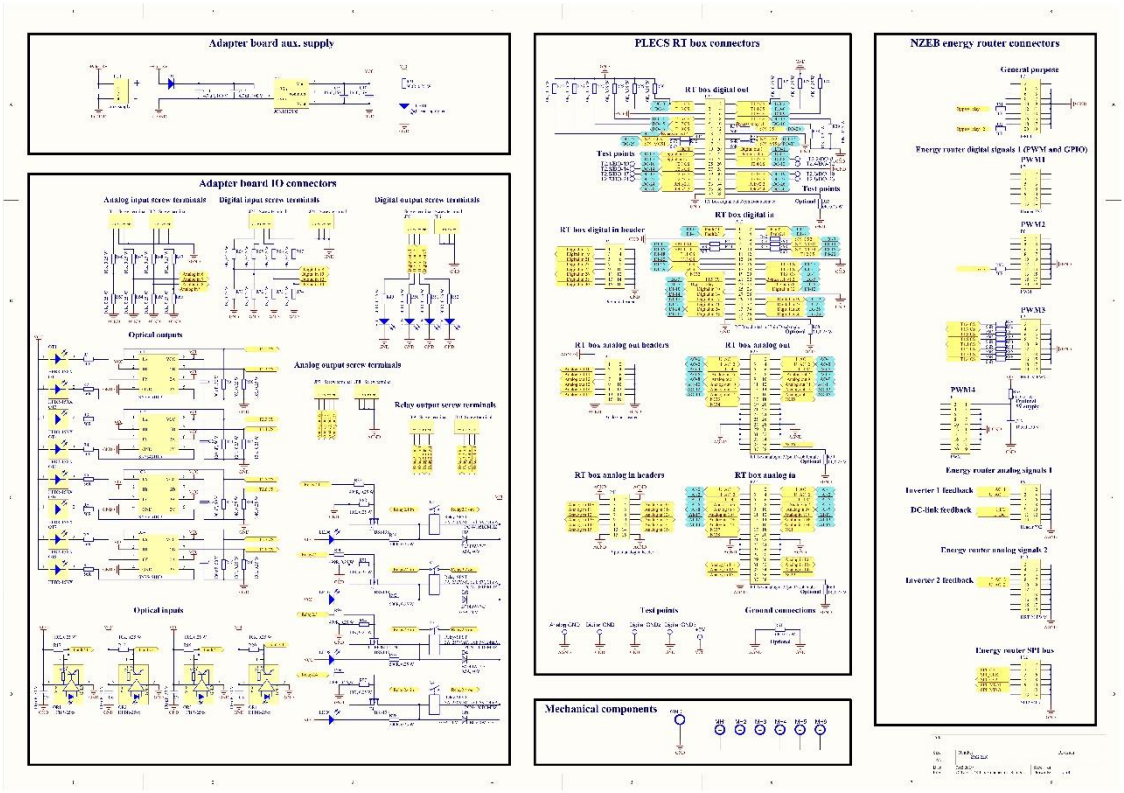

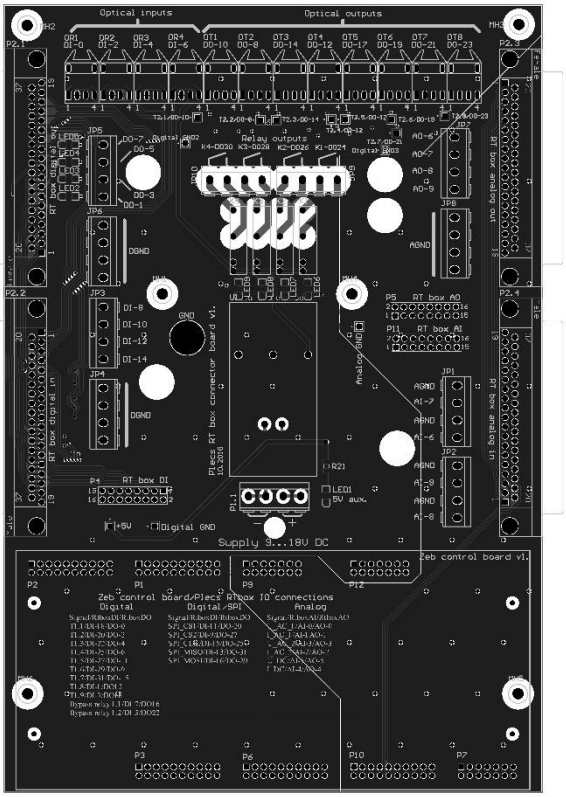

Appendix 3 – Model of Controller

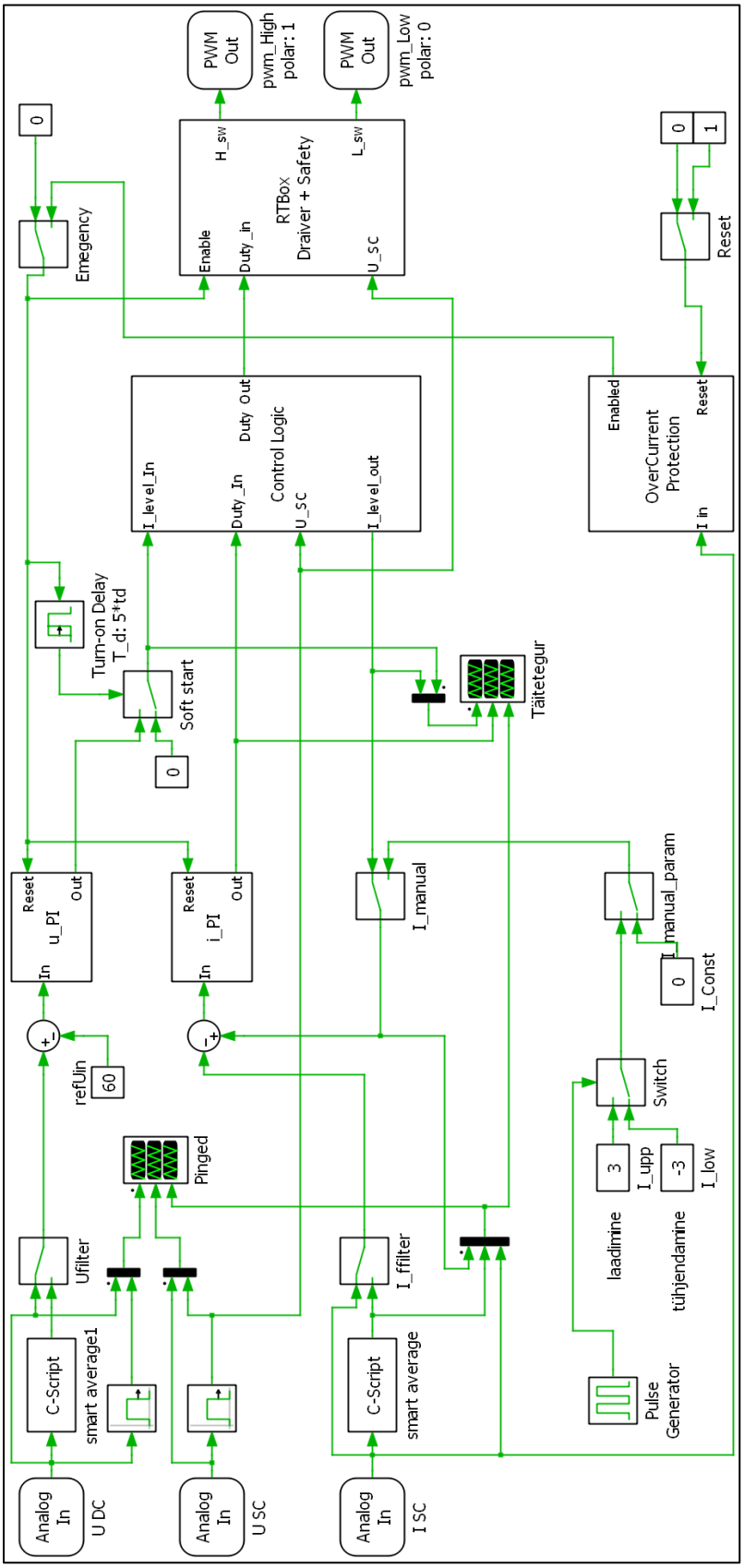

Block “SoC Logic”

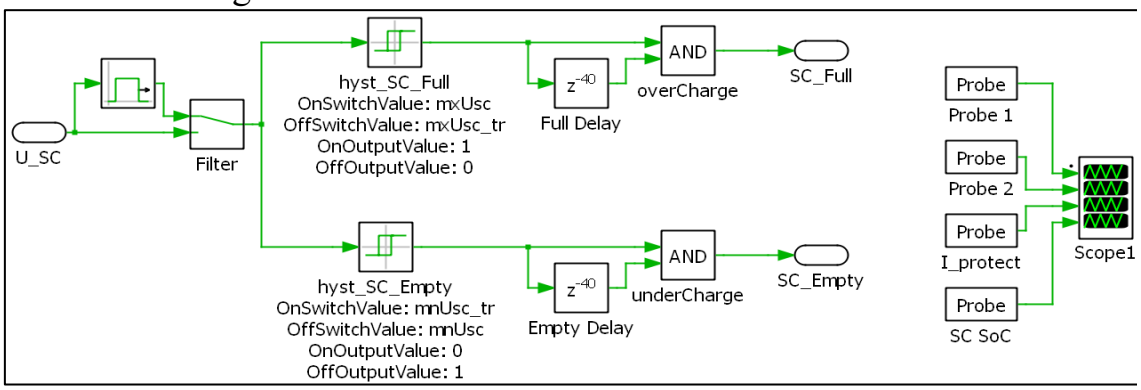

Block “Mode Logic”

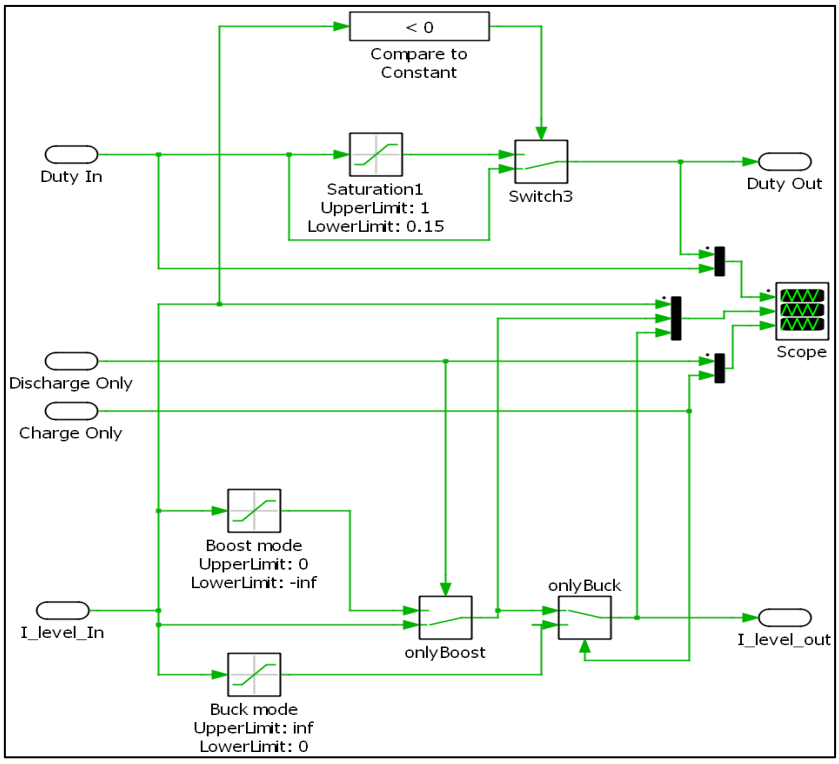

Block “OverCurrent Protection”

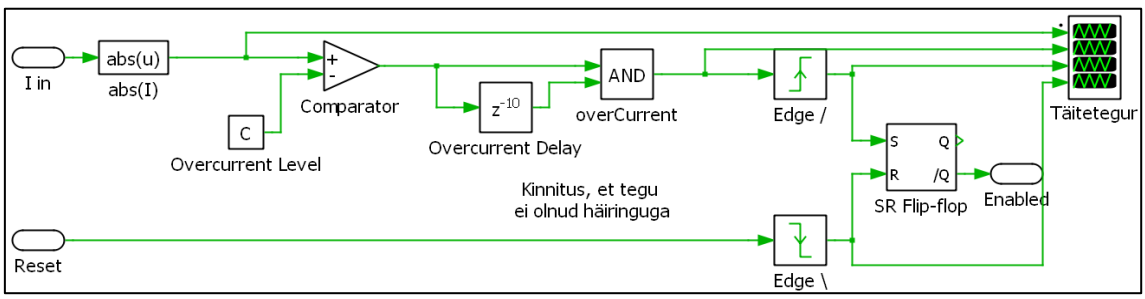

Appendix 4 – BOM

Component	Value	Part Code	Cnt.	unitPric	Source
Current Sensor	50 A	LA 55-P	1	22.44	Farnell
Bridge Rectifier 3-phase	139 A 1800 V	S3PDB180N16	1	28.13	Teval
Capacitor	700 µF 850 V	947C731K801CDMS	1	106.22	Mouser
Capacitor	200 µF 450 V	PPM416.47.0012	1	-	Not availabel
Signali Conditioner		MCR-C-UI-UI-450-DCI	2	~200	Not produced anymore
IGBT Half-bridge module	105 A 1200 V	BSM75GAL120DN2	1	75.42	Mouser
IGBT Driver Module		2SD315AI-33	1	209.7	Mouser
Power Supply	230 VAC 24 V DC 3 A	MPS3-230/24C	1	-	Not availabel
Inductor 3-phase	1 mH	R-3-03K3-AN	1	-	Not availabel
Supercapacitor	165 F 48 V	BMOD0165 P048 BXX	3	~700	used at eBay

Appendix 5 – Test Bench Schematic